Devices and Fibers for Ultrawideband Optical Communications

Devices and Fibers for Ultra-Wideband Optical Communications

Jeremie Renaudier, *Senior Member, IEEE*, Antonio Napoli, Maria Ionescu, *Member, IEEE*, Cosimo Calò, *Member, IEEE*, Gerrit Fiol, *Member, IEEE*, Vitaly Michailov, *Member, IEEE*, Wladek Forysiak, *Member, IEEE*, Nicolas Fontaine, *Senior Member, IEEE*, Francesco Poletti, *Senior Member, IEEE*, Pierluigi Poggiolini, *Fellow, IEEE*,

***Abstract*—Wavelength Division Multiplexing (WDM) has historically enabled the increase of the capacity of optical systems by progressively populating the existing optical bandwidth of Erbium Doped Fiber Amplifiers (EDFA) in the C-band. Nowadays, the number of channels – needed in optical systems – is approaching the maximum capacity of standard C-band EDFAs. As a result, the industry worked on novel approaches such as: use of multi-core fibers; extension of the available spectrum of the C band EDFAs; development of transmission systems covering C and L bands and beyond. In the context of continuous traffic growth, ultra-wideband (UWB) WDM transmission systems appear as a promising technology to leverage the bandwidth of already deployed optical fiber infrastructure and sustain the traffic demand for the years to come. Since the pioneering demonstrations of UWB transmission a few years ago, long strides have been taken toward UWB technologies. In this review paper, we discuss how the most recent advances in the design and fabrication of enabling devices such as lasers, amplifiers, optical switches, and modulators, have improved the performance of UWB systems, paving the way to turn research demonstrations into future products. In addition, we also report on the advances in UWB optical fibers such as the recently introduced Nested Antiresonant Nodeless Fibers (NANF)s, whose future implementations could potentially provide up to 300 nm wide bandwidth at less than 0.2 dB/km.**

***Index Terms*—Optical fiber communication, Ultra-wideband optical communications, Optical components, Lasers, Optical switches, Optical amplifiers, Semiconductor optical amplifiers, Optical fibers**

I. Introduction

THE explosive growth of Internet data traffic and the subsequent demand for cloud services has been a driving force in the evolution of optical networks over a wide range of reaches. This includes subsea, terrestrial long-haul, metro and access as well as data-centers connectivity. The demand for traffic growth, in every segment, is expected to keep thriving because of the forecasted evolution and massive deployment of 5G mobile network, Internet of Things (IOT), cloud computing and storage [1]. These applications have continued to drive up the fiber capacity of modern optical networks, which is economically viable by reducing the cost per bit through the increase in the information payload per wavelength.

Since the first demonstrations of 100 Gb/s coherent systems [2], [3], the Spectral Efficiency (SE) in commercial Wavelength Division Multiplexing (WDM) C-band has significantly increased to sustain the aforementioned ceaseless data traffic growth requirements. Over the past decade, several techniques, such as spectral shaping and high order modulation formats with advanced Digital Signal Processing (DSP), have been introduced to increase the per-wavelength bit rates from the initial 100 Gb/s up to 1 Tb/s and beyond [4], [5]. Significant improvements in Forward Error Correction (FEC) coding allowed the transition from Hard Decision (HD) codes commonly using 7% Overhead (OH) to advanced Soft Decision (SD) codes with higher OHs and better net coding gains [6]–[8]. Nonlinear compensation algorithms have also been proposed to mitigate fiber nonlinear impairments in spectrally efficient advanced transponders [9], [10]. Recently, capacity-achieving constellations, together with low-complexity Bit-interleaved Coded Modulation (BICM) have been introduced to coherent fiber-optic transmission systems [11], [12]. Particularly, Probabilistic Constellation Shaping (PCS) has attracted much attention by allowing the achievable information rate to be tailored to the Signal-to-Noise-Ratio (SNR) region of interest in suitably choosing the Probability Mass Function (PMF) of the constellation points.

However, further improvement of system SE via channel coding innovation is increasingly challenging and comes with diminishing returns as we approach the limit of the nonlinear fiber channel. This limit is unknown to date but is upper bounded by the Shannon capacity formula for the additive white Gaussian noise channel [13], which reads, for dual polarization transmission systems, as

$$C = 2 \cdot M \cdot B \cdot log_2(1 + SNR)$$

where M and B are the number of spatial paths and the optical bandwidth respectively. The SNR is limited by the fiber Kerr nonlinear effect, and its improvement by, e.g., nonlinear compensation, is prohibitively complex [14]. Since the capacity scales logarithmically with the SNR, it is clear that multiplexing techniques represented by the pre-log factors (i.e.

Jeremie Renaudier, Maria Ionescu are with Nokia Bell-Labs France, jeremie.renaudier@nokia-bell-labs.com, maria.ionescu@nokia-bell-labs.com.
Antonio Napoli is with Infinera, UK, London, anapoli@infinera.com.
Cosimo Calò is with III–V Lab, France, cosimo.calo@3-5lab.fr.
Gerrit Fiol is with Fraunhofer-HHI Institute, Berlin, Germany, gerrit.fiol@hhi.fraunhofer.de
Vitaly Michailov is with OFS, New Jersey, USA, vmikhailov@ofsoptics.com.
Wladek Forysiak is with the Aston University, Birmingham, U.K., w.forysiak@aston.ac.uk
Nicolas Fontaine is with Nokia-Bell-labs, New Jersey, USA, nicolas.fontaine@nokia-bell-labs.com
Francesco Poletti is with Southampton University, UK, frap@orc.soton.ac.uk.
Pierluigi Poggiolini is with Politecnico di Torino, Torino, Italy, pierluigi.poggiolini@polito.it.
Manuscript received xxx 19, zzz; revised January 11, yyy.

the number of spatial paths M and the bandwidth B) are best suited to further increase the capacity. Scaling of the number of spatial paths through Spatial Division Multiplexing (SDM) has attracted much attention over the past few years to significantly increase the capacity beyond what Single Mode Fiber (SMF) can offer. The use of Multi-mode Fibers (MMF), Multi-core Fibers (MCF), and their combination, which promise a linear capacity increase scaling with the number of supported cores and/or modes, has been extensively investigated as a solution to meet the future demand for capacity growth [15]–[20]. However, this approach requires the deployment of new fiber infrastructure, the cost of which particularly represents a fundamental practical issue in terrestrial optical networks.

An orthogonal, although complementary, direction to increase the capacity of transmission systems, while maximizing the use of the existing infrastructure, is to extend the bandwidth of the optical amplification beyond what can be offered by the C+L-band Erbium Doped Fiber Amplifiers (EDFA) based approach. This will raise new challenges, e.g., the interplay between fiber Kerr effects and Stimulated Raman Scattering (SRS) combined with the wavelength dependence of system parameters such as fiber loss, Noise Figure (NF) of the optical amplifiers and fiber effective area [21]–[23]. However, the combination of novel extended-bandwidth systems, named here Ultra-wideband (UWB) systems, with the most recent advances in DSP, modulation formats and FECs, would significantly increase the net throughput that coherent WDM systems may achieve [24].

There is more than one approach to realizing UWB and Fig. 1 depicts some of them, as the the different bands – where single mode transmission is possible – can be enabled in different ways.

The first is to design the optimal amplifier per each band. For example, the optimal doping material in C- and L-band is the erbium, while in S-band is the thulium. This approach has the benefit of enabling a pay-as-you-grow principle, so that operators can add bands as needed. In this case, components require to be optimized in a single band [22].

The second option is to develop amplifiers which can cover a larger part of the spectrum, such as Raman amplifier and Semiconductor Optical Amplifier (SOA), in red and green, respectively in Fig. 1. SOAs and Raman amplifiers can cover a spectrum as wide as 100 nm, equivalent to C+L-band system with EDFA, without the need of different doping material. It is worth to mention that bismuth amplifiers, if the material stability could be solved, could cover almost the entire 54 THz from O- to L-band [25]. Here, having optical devices exhibiting good performance over such a wide spectrum would be appealing to fully exploit the benefit of the aforementioned wideband amplifiers, but using different devices covering only part of the spectrum would still be beneficial.

A third and last option is to realize an optical medium, i.e, the fiber, which maintains "good" properties over a wider spectrum. This is the case of hollow-core Nested Antiresonant Nodeless Fibers (NANF), which theoretically might achieve a bandwidth as large as 300 nm while keeping a low-enough attenuation, together with very low non-linearity, low dispersion and lower propagation delay than conventional fibers.

Finally, the different strategies – UWB or SDM with MCF/MMF or parallel fibers, will be selected according to the particular scenarios, e.g., metro/access, long-haul and ultra-long-haul. Apart from the importance of growing traffic, concerns such as losses vary across band types, and therefore also the optimal amplifier and maximum transmission distance will vary.

The remainder of the paper is organized as follows. Sec. II discusses in details the several key-components. Precisely: in Sec. II-A and Sec. II-B we deal with laser and modulators for UWB optical systems, while in Sec. II-C we discuss filter and switches. In next Sec. III, we report on one of the most important elements to enable UWB transmission: the amplifier. Here, we provide a detailed overview on doped fiber amplifier in Sec. III-A, on Raman amplifier in Sec. III-B, and on SOAs in Sec. III-C. The last technical section is devoted to the novel hollow-core fibers of the NANF type. Final Sec. V draws the conclusions.

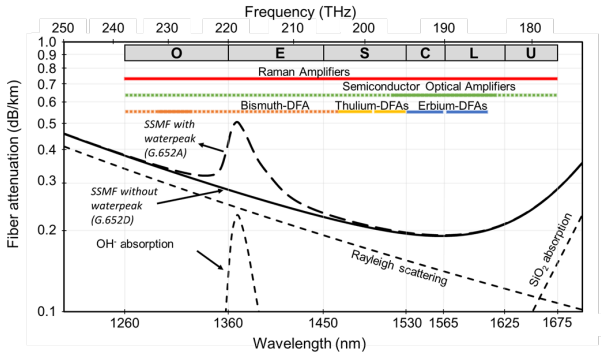

Figure 1: Attenuation over wavelength. The different spectral bands are defined based on ITU nomenclature [26]. Standard Single Mode Fiber (SMF-28) G.652D without OH absorption peak has a bandwidth – with attenuation < 0.4 dB/km – of more than 400 nm.

II. Ultra-Wideband Lasers, Modulators, and Switches

A. Narrow linewidth tunable lasers

Tunable laser sources have become key enabling devices for WDM optical networks, as they allow to fully exploit the optical fiber transmission windows, making efficient use of the wavelength resource in the system. While fixed wavelength lasers are usually preferred for access applications due to cost effective targets, tunable lasers are now massively deployed in most metro and regional/long haul systems in both C and L bands to enable flexibility of wavelength allocations. Therefore the authors believe that system bandwidth extension would also require the development of new tunable laser devices capable of covering those bands, particularly regarding metro to long-haul optical networks. Over the last two decades, extensive research has been carried out on UWB lasers, such as single-wavelength widely tunable lasers and optical frequency comb (OFC) sources. In both cases, the goals have been: to extend the emission bandwidths; to achieve higher output power; and to reduce footprint and lower linewidth to

support high data rate for coherent communications. While OFC sources are highly attractive for multi-Tb/s optical links – as they provide with a single device a multitude of equally spaced channels [27] – their use in telecom system is often hindered by the limited comb spacing tunability and by the need of demultiplexing and externally modulating individual lines prior to transmission. Single-mode tunable lasers are therefore the preferred choice for flexible and future-proof UWB optical networks. In this section, we will outline the landscape of existing solutions for single-wavelength widely tunable lasers in the C- and C+L-bands and discuss trends and challenges for the development of such key devices.

The literature on wavelength tunable lasers is extraordinarily rich and a wide variety of configurations and tuning mechanisms have been proposed (see e.g., [28] for an in-depth review). Among the various approaches, Indium Phosphide (InP) Photonic Integrated Circuits (PICs) have received considerable attention in the past, owing to their compact size and the exploitation of well-established III–V manufacturing technology, allowing to monolithically include on-chip SOAs to boost the output power of the tunable laser and/or to suppress the laser output during wavelength tuning. Wavelength-selectable sources – based on Distributed Feedback (DFB) or Distributed Bragg Reflector (DBR) laser arrays [29]–[32] and sampled- or super-structure gratings DBR lasers [33], [34], in particular – have reached commercial maturity in the Integrated Tunable Laser Assembly (ITLA) market. These types of sources can provide large output power (>20 mW) over the C- or L-band, as well as wavelength tuning ranges exceeding 40 nm, depending respectively on the number of devices in the array and on the grating design. Yet, achieving optical linewidths below 200 kHz with monolithic InP tunable laser can be challenging, mainly because of the large absorption losses in InP waveguides that reduce the laser intracavity power.

A well-known strategy for narrowing down the optical linewidth is to design the laser cavity to increase the photon lifetime [35]. This can be obtained, for example, by including a semiconductor gain element within a low-loss extended cavity comprising a passive tunable filter. Such an External Cavity Laser (ECL) approach has become, in recent years, the preferred way of realizing widely tunable sources for coherent communication systems. In most common implementations, ECLs with high output power and ultrawide tunabilities are achieved by coupling Reflective Semiconductor Optical Amplifier (RSOA) chips with free-space filtering elements, such as Fabry-Perot (FP) etalons or diffraction gratings (typically in Littrow or Littman-Metcalf configuration). In [36], for example, a device with a tuning range in excess of 130 nm has been demonstrated using an FP etalon and an intra-cavity acousto-optic tunable filter. Unfortunately, laser assembly approaches – employing discrete optical elements – often exhibit large footprints, which may prevent the packaging of these sources in standard modules for telecommunication applications.

The recent trend towards the realization of compact narrow-linewidth widely tunable lasers is to build laser cavities by coupling one or more III–V semiconductor gain sections to a tunable filter PIC fabricated in a low-loss material platform like SiO_2, Silicon Nitride (SiN) or Silicon-on-insulator (SOI). In several cases, the PIC makes use of a thermally tuned Vernier Microring Resonator (MRR) filter that effectively allows to extend the laser cavity for optical linewidth reduction, without making compromises on the device footprint. A summary of the state-of-the-art of MRR-based ECLs with the widest tuning ranges is reported in Table I and discussed hereafter.

Among the different device implementation strategies presented in the literature, one of the most effective to tune wavelength range, output power, and optical linewidth is the hybrid integration approach, where separately optimized passive PICs and III–V gain chips are butt-coupled or assembled together on a common micro-optical bench platform to build the laser cavity. Fig. 2 illustrates this approach recently demonstrating hybrid InP-SiN microring-resonator based tunable laser with high output power and narrow linewidth for high speed systems [37]. In [38], ECL designs with record tunabilities up to 160 nm have been demonstrated using silica Vernier filters consisting of the series connection of up to three MRRs and an on-chip mirror. The same authors have later reported on similar devices, with tuning ranges up to 96 nm and fiber-coupled power in excess of 13 dBm, using flip-chip mounted RSOAs for mass production purposes [39]. In [40], a UWB-RSOA with 3 dB gain bandwidth of 120 nm is employed in combination with a SOI PIC, which consisted of a MRR, an Asymmetric Mach-Zehnder Interferometer (AMZI) and a Sagnac Loop Mirror (SLM), in order to build a compact widely tunable ECL. The device exhibits a 550 kHz linewidth, 20 mW of fiber-coupled output power and a tuning range of 95 nm, primarily limited by the Free Spectral Range (FSR) of the SOI filter. More recently, the use of ultralow-loss SiN PICs has allowed the demonstration of state-of-the-art ECL performances, especially in terms of optical linewidth. In [41], the authors disclose different laser designs respectively optimized for broadband tunability (120 nm tuning range), high output power (105 mW fiber-coupled), and record-low linewidth (down to 40 Hz). The widest tunability in this work is obtained by adding a suitably designed AMZI to a two-MRR Vernier filter, in order to nearly double the FSR of the latter and, at the same time, control the laser output power.
Although hybrid integration typically implies high inherent costs for chip-level alignment and testing, the possibility of automatizing the assembly process, e.g., through optimized flip-chip bonding of III–V gain chips on silicon photonic platforms [39], [42], [43], is a major driver towards large-scale industrialization of high-performance ECLs.

While the ultimate solution for monolithically integrating low-cost and large volume semiconductor lasers on silicon photonics platforms would be the direct growth of III–V materials on Silicon (Si), this approach appears to be too challenging for practical applications. Therefore, methods like wafer/die bonding and micro-transfer printing have received particular attention for the prototyping and possibly large-scale manufacturing of devices integrating III–V elements on SOI and SiN platforms. These heterogeneous integration approaches have already enabled the demonstration of state-of-the-art lasers [35], [44], [45], as well as UWB tunable sources. Most notable examples of the latter include the InP/SOI laser

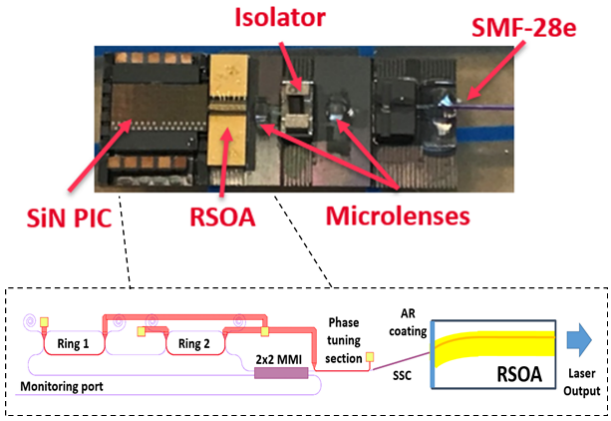

Figure 2: Micrograph picture and schematic of high power hybrid InP/SiN microring-resonator based tunable laser [37].

reported in [46], exhibiting a tuning range of 90 nm and output power up to 9 mW, or the device demonstrated in [35], employing an SOI filter composed of 4 MRR within an SLM to achieve a tuning range of 120 nm and an optical linewidth of 140 Hz.

Regardless of the integration strategy, hybrid or heterogeneous, the microring-based ECL paradigm [35], [41] is promising for achieving ultrawide tuning ranges. This approach is at the same time wavelength- and photonic integration platform-agnostic, thus several possibilities exist to build UWB sources in other bands of interest than C+L, through bandgap engineering of the III–V active material and suitable filter PIC design. Moreover, the recent advances on SOI and SiN integrated photonics, as well as on emerging platforms like Lithium Niobate on Insulator (LNOI), pave the way towards the realization of complex PICs possibly combining widely tunable lasers with fast on-chip modulators and other UWB functions.

B. Optical Modulators

Various types of modulation techniques have been implemented in optical communication. Among them, the common ones are directly modulated lasers, electro-absorption modulators, and intensity/phase modulators employing a Mach-Zehnder Interferometer (MZI) configuration. If it comes to electro-optic modulation bandwidth and higher order modulation formats (e.g., modulation of intensity and phase), Mach-Zehnder Modulator (MZM) represents the right choice and will be discussed in the following. The commonly used structure is a (Dual) IQ-Modulator, which consists of two Mach-Zehnder Modulators nested in a parent waveguide structure, while for the Dual-IQM, two IQMs are placed on one chip to handle two polarizations.

Historically, bulk Lithium Niobate ($LiNbO_3$ – legacy LN) modulators were widely used in long-haul transmission for decades. Thanks to the wide range of transparency of Lithium Niobate, legacy LN modulators are commercially available for center wavelengths ranging from 635 nm up to 1577 nm [47]–[49]. Semiconductor modulators mainly made of InP, Gallium-

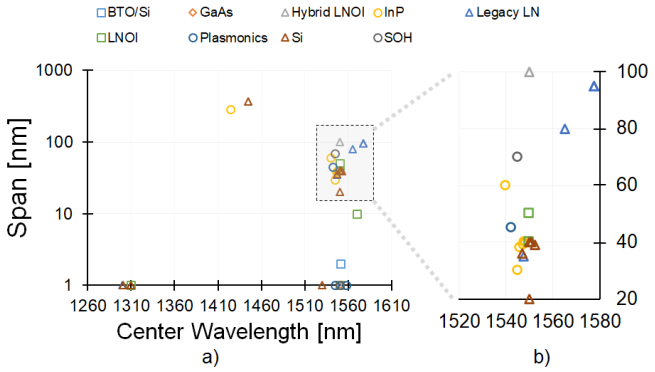

Figure 3: **a)**: published optical bandwidth of MZM for various phase-shifter materials (taken from references [66] for BTO/Si, [67]–[70] for hybrid LNOI, [47]–[49], [71] for legacy LN, [55]–[57] for Plasmonic, [59], [72], [73] for SOH, [50], [74]–[76] for GaAs, [51], [52], [54], [77], [78] and this work for InP, [61], [63], [79]–[82] for LNOI and [83]–[92] for Si). The published operation wavelength ranges have been recalculated to a center and span value and the published span values <1 nm have been artificially set to 1 nm to enhance visibility. **b)**: Inset to show the C-band enlarged.

Arsenide (GaAs) and Si have emerged because they are attractive in terms of size, higher modulation rates and lower drive voltages, along with associated power consumption [50]–[54]. Those modulators usually have to be operated well above the band edge to minimize optical absorption. Recently, Polymer, Plasmonics and Silicon-organic hybrid (SOH) modulators are reported [55]–[60] as well as thin film Lithium Niobate (TFLN) [61]–[65]. Note that for most of the modulators, results are presented in the literature for a single wavelength or wavelength range spanning a few 10 nm.

Fig. 3 shows the retrieved center wavelength and operation span from published works. Start/Stop operation wavelength published are recalculated to center/span values. Here, no further filters, e.g., e.g., maximum have-wave voltage (V_π), loss or minimum electro-optic modulation bandwidth are applied. If no operation wavelength span is given in the publication, it is set to 1 nm to allow a clear visualization in Fig. 3. The commonly used C-band centered around 1550 nm is plotted enlarged on the right-hand side of Fig. 3. Span values here are mostly $\sim$40 nm, so that these devices can cover the entire C-band. A Si based optical modulator is reported to work over 370 nm [90] while in Fig. 4 it is shown for an InP modulator with 288 nm span.

For a modulator, several building blocks have to work over the desired wavelength range, namely phase shifters, splitters/combiners (e.g., Multi-mode Interference (MMI), Y-Splitter) and coupler from/to the chip (e.g., taper structure or gratings). Phase shifter efficiency depends on the underlying nature of the electro-optic effects present (Pockels, Franz-Keldysh, Plasma, or Quantum-Confined-Stark Effect), it has different overall strength and may vary with wavelength. Values range from 0.006 V·cm for Plasmonic modulators to as large as 20 V·cm for legacy LN modulators [64]. However, one has to keep in mind that the figure of merit should include the phase shifter loss as well as modulation bandwidth [64], [93].

InP modulators rely on the Quantum-Confined-Stark Effect,

Wavelength [nm]	**Output power** [mW]	**Tunability** [nm]	**Linewidth** [kHz]	**Co-integration with Si photonics**	**Ref.**
1475 – 1635	2.5 / 20	160 / 96	500	Hybrid	[38], [39]
1540 – 1635	20 / 10	95 / 66	550 / 1	Hybrid	[40]
1480 – 1600	24 / 105 / 1	120 / 100 / 70	2000 / 320 / 40	Hybrid	[41]
1546 – 1636	9	90	N/A	Heterogeneous	[46]
1500 – 1620	2	120	140 [Hz]	Heterogeneous	[35]

Table I: State of the art of microring resonator based tunable lasers with widest tuning range.

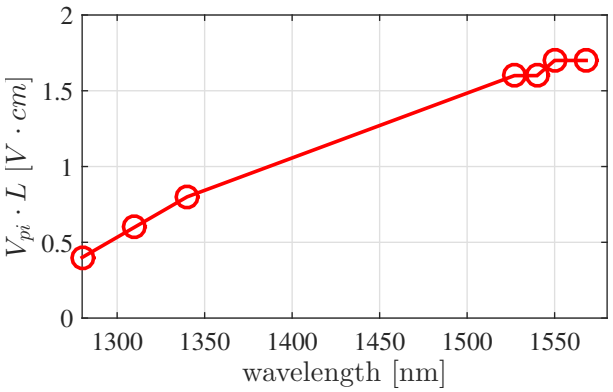

Figure 4: Figure of merit Vpi·L calculated from measured V_π values for an InP-MZM originally designed to work in the O-Band. The 3 dB bandwidth of the electro-optic response of this device was measured to be 43 GHz. The dashed line represents the interpolation between O- and C-band, as those values could not be assessed due to setup limitations.

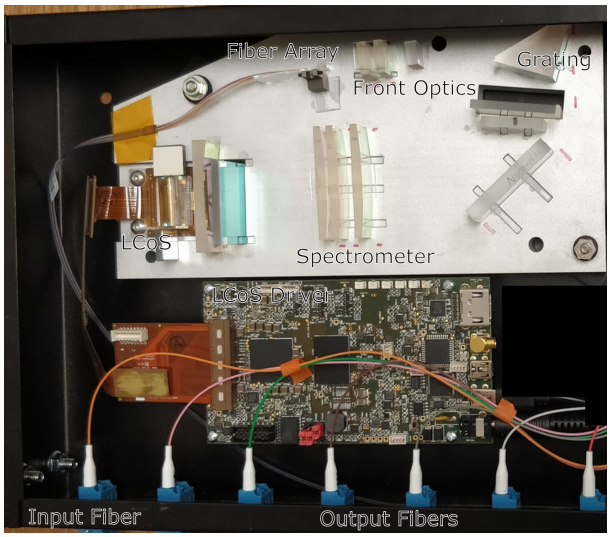

Figure 5: Typical UWB-WSS including fiber array, freespace optics, grating, LCoS, LCoS Driver and the input and output fibers.

therefore the phase shifter efficiency is varying with wavelength. However, as it can be observed from Fig. 4 the value range from 0.4 V·cm at 1280 nm to ∼1.8 V·cm at 1567 nm, with the highest value of ∼1.8V·cm still being comparable or lower than most of the published work on Si, GaAs, TFLN and legacy LN [64]. Furthermore, the device in Fig. 4 shows 43 GHz 3 dB EOR bandwidth.

Splitters/Combiner are needed to form an interferometer. Common implementations are MMIs, Y-branches or directional couplers. The most important parameters are induced Insertion Loss (IL) and Splitting Ratio (SR), with the latter having a direct impact on the extinction ratio and subsequently on the performance of the IQM [94]. 1×2 MMI and Y-branches, used for splitting the light, have wavelength independent SR. Common 2×2 MMIs used for recombining the light have wavelength dependent SR with recently published sub-wavelength grating structures, where this effect is leveraged [95]. If it comes to process sensitivity, MMIs are generally preferred.

Coupling the light efficiently from the fiber to the chip and vice versa is needed to keep the IL low, in the best case, with mode sizes matching to cleaved single-mode fibers allowing good alignment tolerances. While horizontal tapers can be realized by appropriate mask and etching, vertical tapers can be either realized by etching or enhanced regrowth techniques. Regrown tapers in InP yield an almost symmetrical spot, and work as long as the band edge of the light guiding layer is sufficiently lower than the operation wavelength. Grating structures usually have a limited wavelength range.

C. Optical filters and switches

The primary wavelength routing devices in optical networks are Optical Cross Connect (OXC) [96] and Wavelength Selective Switch (WSS) [97], [98]. OXCs are N input N output devices where the entire waveband is switched simultaneously between pairs of input and output fibers. If they are built using Micro-Electro-Mechanical Systems (MEMS) mirrors, these devices are inherently broadband.

WSSs are typically single input devices with multiple outputs, where each wavelength on the input port can be routed to an output port. Typically, additional functionality of WSSs such as spectral attenuation, can be used to equalize channel plans. The switching element inside most WSSs are Liquid Crystal on Silicon (LCoS) spatial light phase modulators and currently have approximately 2000 pixels in the wavelength direction and 1000 pixels in the steering dimension, which allow for approximately 100 GHz, 50 GHz spaced channels with two 1×32 switches placed inside one box.

Fig. 5 shows the insides of a typical WSS. WSSs are primarily free-space optics devices because they need to use all 3 spatial dimensions. Out of the two orthogonal transverse spatial dimensions, one is used to steer the light to different ports, and the other is used to separate wavelengths. The optics inside a WSS are typically cylindrical, with horizontal optics used for wavelength separating and vertical optics used for steering. The operation of the switch is as follows. First, light enters the WSS on a fiber array and the beams are collimated using micro lens arrays. The front optics then reshape the beams to fit as many separated spots vertically on the grating and, in the horizontal axis, expand the beam to fill as many grating lines

as possible. The spectral resolution is inversely proportional to the number of grating lines illuminated. Because the grating and LCoS are polarization sensitive, the front optics include polarization diversity optics to separate both polarizations such that they take different spatial paths through the WSS and are properly recombined at the output port. After the grating, the spots are "Fourier transformed" from the grating onto the LCoS through a series of lenses in the spectrometer. In the vertical direction, the spots are spatially overlapped on the LCoS but each spot hits the LCoS with a slightly different angle. Sawtooth holograms (i.e., linear phase) can steer light from one port to another. In the horizontal direction, the wide spots on the grating are focused to a narrow spot, where each wavelength focuses to a different horizontal location. Since the wavelengths are spatially separated, the LCoS can apply separated steering to each wavelength.

The simplest way to realize broadband WSSs is to change the spectrometer optics. One technique would be to use a less dispersive grating, or to shorten the focal length of the wavelength spectrometer optics. In [99], the authors used a grating bonded to a prism (GRISM) to modify the spectral dispersion and to build a WSS supporting 15 THz of bandwidth around 1550 nm. Clearly, the spectral resolution will typically decrease proportionally to the increase in spectral bandwidth. Further extension of UWB WSS operation has been reported in [100] demonstrating a 9-port WSS with MMF interfaces supporting approximately 36 THz of bandwidth ($\sim$1 μm), in which the grating had significantly less dispersion. Recently, as depicted in Fig. 6, the authors of [101] demonstrated a 48-port WSS spanning parts of the O-band to the end of the C-band with low enough loss that it could be used to equalize and combine multiple wideband components.

III. Ultra-Wideband Optical Amplifiers

A. Doped Fiber Amplifiers

The advent of EDFAs was a fundamental breakthrough for optical communications, not only for the first deployments of optical systems in the early nineties, but also for the development of high capacity optical networking carrying some Tb/s data based on wavelength division multiplexing. This technology is the most matured amplifier technology and provides gain over the "conventional" C-band (1530–1565 nm) as well as part of the "long" L-band (1565–1625 nm). Combining C- and L-band EDFAs, remarkable transoceanic transmission experiments were reported with throughputs closely approaching capacity limits [102], [103]. Note that it has also been reported that L-band amplification bandwidth can be further extended using Bismuth or Bismuth-Erbium doped fiber amplifiers [104], [105]. Commercially available EDFAs are based on a few tens of meters of doped fiber and can provide over 20 dB of gain with typical NF as low as 4.5 dB. However, EDFAs cover only one fifth of the SMF low-loss bandwidth of 54 THz. Over the past decades, there were considerable efforts to develop doped fiber amplifier solutions for the remain parts of the optical spectrum.

"Short" S-band (1460–1530 nm) is adjacent to C-band, which makes it attractive to extend the amplified transmission bandwidth since relatively small effort is required to redesign optical components (e.g., lasers) and subsystems like Reconfigurable Optical Add and Drop Multiplexing (ROADM)s. It has been demonstrated that Erbium doped fiber (EDF) can be used to boost optical signals over the long wavelength part of S-band (1490–1515 nm). However, this solution requires the use of multiple stages with gain tilt control filters. The amplifier demonstrated in [106] had the total 43 m of gain fiber that has been split by 6 filters between 8 stages, and it delivered 21 dB gain with 6.7 dB of NF. Alternatively, Thulium doped fiber can be used to amplify signals over 1480–1510 nm bandwidth with 22 dB gain, and less than 6 dB NF [107]. Although such characteristics are not as good as those provided by EDFAs, Thulium doped fiber amplifiers have been recently proposed to further increase optical transmission bandwidth beyond C and L bands, and boost the total throughput in short distance scenarios [108]. However, this amplifier requires a fluoride ZBLAN (the acronym originated from ZrF_4-BaF_2-LaF_3-AlF_3-NaF composition) host glass with a melting temperature of between 200 and 300 degree, more than one order of magnitude lower than conventional optical fibers. This melting temperature difference makes it impossible to splice ZBLAN and glass fibers using arc fusion splices.

"Extended" E-band can be amplified almost entirely by neodymium doped microstructure fibers (1360–1460 nm) and the amplifier with the gain of 20 dB and NF of 5 dB has been demonstrated [109]. Recently, Bismuth-Germanium co-doped fiber has been developed to provide amplification over the 1410–1450 nm range with the performance and parameters similar to commercially available EDFAs [110]. Notable advantages of Bismuth doped fibers are the silica host glass, similar to commonly used SMF and EDF and conventional manufacturing Modified Chemical Vapor Deposition (MCVD) manufacturing process which simplify splicing and production, compared to non-silica or microstructure fibers.

"Original" O-band (1260–1360 nm) which is centered around zero dispersion wavelength of a SMF fiber may look attractive for capacity increase since it has been extensively used for point-to-point transmission and therefore a large family of optical components has been developed over the past decades. In the late nineties Praseodymium doped fiber amplifiers (PDFA) have been proposed to provide amplification over 1290–1315 nm part of O-band with the gain up to 22.5 dB [111], [112]. However, due to ZBLAN host glass, these amplifiers require mechanical splices which increases the NF up to 6.5 dB and limits their application to the test and measurement field.

It has been demonstrated that Bismuth doped phosphosilicate fiber can amplify almost the entire O-band and a variety of bismuth doped fiber amplifiers (BDFAs) have been developed [105], [113]–[115] with gain as high as 30 dB and NF as low as 5.2 dB. It should also be noted that, unlike PDFA, single stage BDFA can operate over the IEEE standardized part of O-band (1268-1310 nm) [115] which is important for BDFA deployment. Although these amplifiers demonstrated performance similar to commercially available C-band EDFAs, the required doped fiber length is 3–4 times longer compared to typical EDFAs and the highest reported power conversion

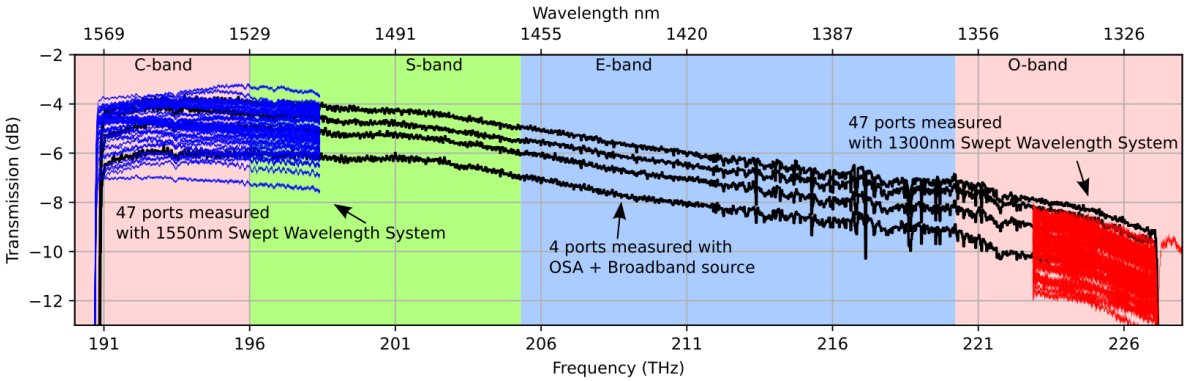

Figure 6: 36-THz bandwidth WSS insertion loss summary presented in [101] The black curves indicate measurements of 4 ports using a broadband source and an OSA. The blue and red curves represent 47 port measurements using 2 swept wavelength systems at 1300 nm and 1550 nm, respectively.

efficiency is limited by 20%.

In addition to transmission bands with wavelengths shorter compared to C-band, there is U-band (ultra-long wavelength) that lays between 1625 nm and 1675 nm where, to the best of our knowledge, fiber amplifiers have not yet been developed. Above 1700 nm the loss of conventional optical fibers rapidly increases which make amplified transmission over this wavelength range impractical. However, as it is stated in the next section of this paper, Hollow Core Fiber Technology (HCF) and, to some extent NANF, can further extend the low loss window. It should also be noted that, compared to glass core fibers HCF have notable advantages of very low nonlinearity and 33% lower latency that makes them attractive for certain applications. Thulium fiber can provide gain in this wavelength range using commercially available fiber (OFS TmDF200^{TM}) designed for non-telecom fiber lasers and amplifiers. It has been demonstrated that 12–16 meters of TmDF200^{TM} can provide 30–35 dB gain with noise figure lower than 6 dB in short (1910–1970 nm) and long (1970–2020 nm) wavelength configurations [116].

In summary, the standardized wavelength bands of the low loss bandwidth of SMF can be amplified using doped fiber amplifiers since there are two dopants available for providing amplification. Most of these amplifiers allow gain, NF and, output power similar to commercially available EDFAs. Properties and parameters of doped fiber amplifiers reviewed in this section are summarized in Table II. However, some of these doped fibers have very different properties compared to SMF-28 or even EDF, which makes their manufacturing and connection to SMF complicated. A family of Bismuth doped fiber amplifiers operating over O- E- and L- bands may be seen as prospective candidates for amplified transmission beyond C- and L- bands since BDF have the same silica host glass and manufacturing process similar to SMF and EDF. Recently, BDF amplifiers, capable to amplify signals over O-band local area network (LAN)-WDM and CWDM standardized wavelength ranges of 1272-1310 nm and 1265-1320 nm respectively, have been introduced to the market [117]. Typical gain and noise figure of such LAN-WDM tailored amplifiers are shown in Fig. 7. BDF amplified O-band may be considered as a next step to increase the lightwave system capacity since O-band BDFA has 17.4 THz bandwidth, more than 1.5× higher compared to C- and L- bands EDFAs combined, and O-band optical component ecosystem is well established.

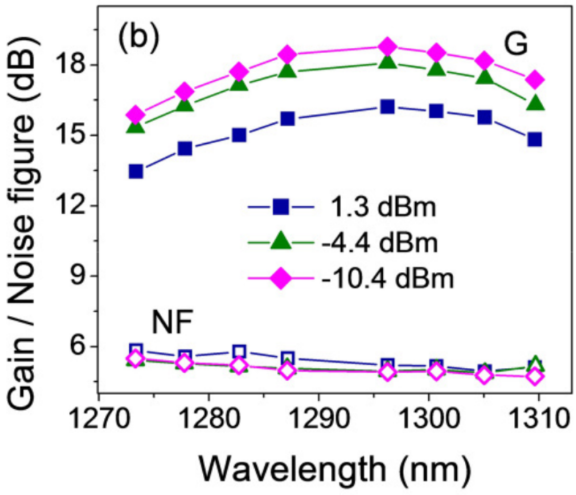

Figure 7: Example of gain(G) and noise figure (NF) of single stage BDFA optimized for LAN-WDM wavelength allocation [117].

B. Raman amplifiers

Both EDFAs and Raman amplifiers have been the subject of intense research since early 1980s [118]. The race between EDFAs and Raman amplifiers favored the adoption of EDFAs as of the early 1990s. The primary reason for the slowing interest in Raman amplification was, at the time, the lack of high-power pumping technology, a primary requirement to provide gain through SRS. Another impediment was the lack of pumps at the required wavelengths, such that maximum SRS efficiency could be provided in the transmission window of the lowest-loss region of silica fiber, of early conventional band systems.

Nevertheless, distributed Raman amplifiers have found widespread commercial application over the years [118],

Band (nm)	BW (nm)	Dopant	Fiber	L (m)	G (dB)	NF (dB)	P_o (dBm)	Amplifier design	Refs.
S:	1490-1515	Er	Silica	43	21	6.7	17.9	8 stages with 6 gain flattening filters	[106]
1460-1530	1480-1510	Tm	ZBLAN	13	22	6	N/A	Single stage, symmetrically pumped	[107]
E:	1380-1440	Nd	μ-structure	14	20	5	23	Two stages, symmetrically pumped	[109]
1360-1460	1410-1450	Bi+Ge	Silica	80	20	7	16	Single stage, symmetrically pumped	[110]
O:	1290-1315	Pr	ZBLAN	24	22.5	6.5	16	Two stages, co- counter pumped	[111], [112]
1260-1360	1268-1360	Bi+P	Silica	80-150	20	5.5	16	Single-stage counter pumped	[113], [114]
U+: 1970-2020	1970-2020	Tm	Silica	12-16	30	6	30	One/Two stages co- counter pumped	[116]

Table II: Summary of doped fiber amplifiers. Legend: BW – bandwidth; L – length; G – gain; NF – noise figure; P_o – output power.

[119], initially in long-distance single-span unrepeated transmission, where distributed Raman amplification (even with multiple-order pumping) provides improved NF [120], and more recenty to a greater extent in conventional long-haul systems to support the higher OSNR requirements of advanced modulation formats [121]. Depending on the span configuration, distributed Raman amplification can be implemented via forward-pumping and/or backward-pumping ~~, or as a remotely-pumped optical amplifier (ROPA)~~, as shown in the schematics of Fig. 8. Backward-pumping configurations are preferred to forward-pumping configurations due to the lower NF and higher stability with respect to the relative intensity noise of the pump sources [122]. Leveraging current generation pump components, C+L-band EDFAs can achieve an aggregate ∼75 nm bandwidth with a band gap between the C- and L-bands [123]. The Raman gain window in silica core single mode fibers, on the other hand, typically exhibits a gain peak at about 13 THz shift from the pump wavelength [124], corresponding to around 100 nm shift at usual telecommunication wavelength bands, as shown in Fig. 9 for a pump wavelength at 1450 nm. Since the Raman gain spectrum shifts with the pump wavelength, it is common to use multiple pumps with advanced tailoring of the spectral shape to generate a flat and wide gain bandwidth. Moreover, since SRS gains depend only on the wavelength difference between the pump and the signal, Raman amplifiers can be built for any bandwidth of interest, beyond the conventional 1530 nm – 1610 nm range. ~~is shown in Fig. 9, measuring the gain peak at 100 nm shift from the pump wavelength here at 1450 nm. The gain spectrum shifts with the pump wavelength. It is common to use multiple pumps to provide Raman gain, thus enabling advanced tailoring of the spectral shape, but for an added complexity. Moreover, since SRS gains depend only on the wavelength difference between the pump and the signal, Raman amplifiers can be built for any bandwidth of interest, beyond the 1515 nm – 1615 nm range.~~

In the context of UWB systems and networks, the highly flexible spectral characteristics of Raman amplifiers, which are mainly determined by the availability of suitably high power pump lasers of appropriate wavelength, offer the potential for multiband or even seamless UWB Raman amplification, either when deployed in their own right, or in concert with the established C-band, or C+L band EDFAs. One key challenge for the operation of UWB Raman amplifiers is to generate and control the desired gain profile in the presence of the significant nonlinear interactions across the spectral band. To this end, various computational techniques have been

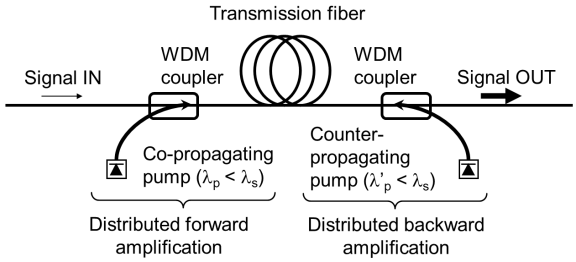

Figure 8: Schematic of distributed Raman amplified system, including forward and backward pumping configurations ~~and ROPA~~.

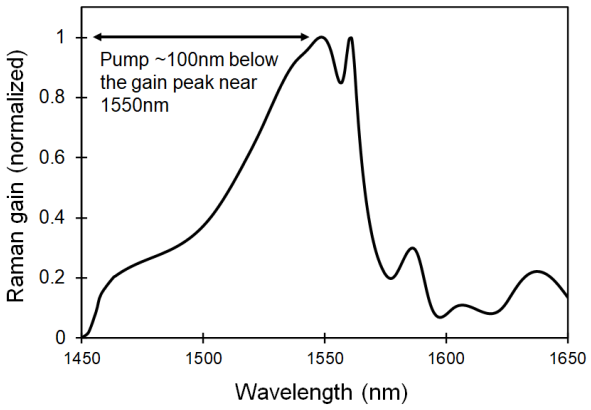

Figure 9: Raman gain spectrum around 1550 nm for a SMF-28 using a laser pump at 1450 nm [124].

applied to this inverse problem over the years, including genetic algorithms. More recently a new class of machine learning techniques has been explored to learn the complex pump-signal relations in this more complex type of Raman amplifier [125]. As illustrated in Fig. 10, once trained, such an approach can support fast and reliable provision of a range of UWB arbitrary gain profiles in a controlled way, thus enabling the potential elimination of static and lossy gain flattening filters, and well as signal power spectrum shaping to facilitate the maximization of the achievable information rate in UWB systems as described in Section III. Further advances in the NF prediction and the optimization of hybrid EDFA-Raman C+L band amplifiers, leading to significant decrease of gain ripples have been reported recently [126], [127], techniques which are expected to also apply to the equally complex multi-stage UWB DRAs described in the second half of this section.

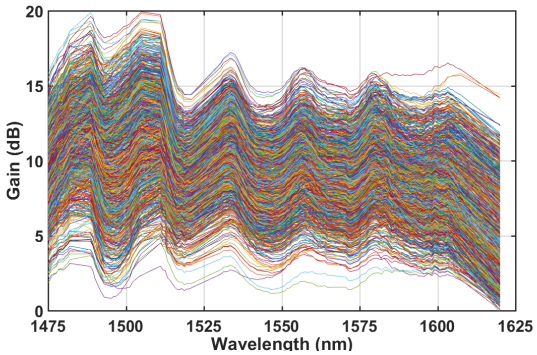

Figure 10: Measured gain profiles for various pump configurations, with pump wavelengths at [1365, 1385, 1405, 1425, 1445, 1465, 1485, 1508] nm, and pump powers limited to 27dBm per wavelength [125].

Raman amplification used in hybrid implementations has been often preferred to achieve remarkable transmission results with EDFA [128], [129] and recently SOAs [130], [131], by relaxing the requirements on the pump powers, while providing continuous gain at low NF. Similarly to SOAs [132], Raman amplifiers can cover all bands and are technology-ready, thus making them as attractive as the highly specialized doped fiber amplifiers for bands beyond C+L. One of the main benefits of Raman amplifiers over doped fiber amplifiers is the potential to achieve continuous wideband transmission of up to 100 nm for the same Optical Signal-to-Noise-Ratio (OSNR), or alternatively, increase the OSNR over the same transmission bandwidth, due to its operation at a lower NF [119]. This benefit is leveraged for instance in the experimental setup depicted in Fig. 11 combining UWB SOA at the transmitter and receiver ends with backward-pumping distributed Raman amplification to demonstrate a 100 nm wide unrepeated transmission system. Second order backward Raman pumping using pumps at 1365 nm, 1425 nm, 1455 nm and 1494 nm, provided average Raman on-off gain of approximately 28 dB, typical of unrepeatered links. Such UWB hybrid amplification scheme enabled 140% increase in capacity $\times$ distance product for unrepeated transmission systems [131].

Raman amplifiers can be deployed under multiple configurations depending on the targeted system, primarily suited for unrepeatered transmission, short-distance subsea or long-distance terrestrial systems. Differences between the deployment of Raman in submarine systems compared to terrestrial systems are considerable from the power consumption point of view. Since submarine systems are electrical power limited, these limitations translate inversely into achievable transmission distances. Short repeteared as well as unrepeatered subsea systems based on Raman amplification have already been commercially deployed [133], [134]. However, the current challenge for energy efficiency hinders the adoption of Raman amplification from long-haul submarine transmission [135] and places SDM as a strong competitor to ultra-wideband amplifiers [136]. On the other hand, long-haul terrestrial systems can benefit from Raman amplifiers, since the electrical power limitations are relaxed compared to subsea systems. Metro networks pose additional challenges in configuring discrete, or lumped, Raman-based amplifiers where all amplifier elements are located at the amplifier node, as ROADMs dynamically change the gain requirements across the bandwidth.

The Raman effect can be also exploited to realize discrete Raman amplifiers (DRA), which do not provide the NF benefits of distributed amplification, but are functionally equivalent to a conventional EDFA. This kind ~~type~~ of amplifiers enables the use of specialized nonlinear fiber as the Raman gain medium, leading to increased pump efficiency, and has the added safety benefit of not requiring pump light in the operator's fiber plant. Fig. 12 shows a schematic diagram of a dual-stage DRA consisting of three pairs of first-order pump laser diodes in the first stage (1365 nm, 1385 nm, and 1405 nm), followed by five pairs of diodes in the second stage (1425 nm, 1445 nm, 1465 nm, 1485 nm, and 1508 nm) [137]. The 8 Raman pumps are distributed over the two stages in this way to inhibit the strong pump-to-pump Raman energy transfer that would take place in an equivalent single-stage amplifier, and to improve the short-wavelength NF [138]. Hence, the first stage provides gain for the S-band signals, while the second stage provides gain for the C+L band signals, with an overall gain of $\approx$15 dB and an NF no worse than $\approx$8 dB at any point in the transmission band extending from 1475–1625 nm [137], as shown in Fig. 13. The NF is low at short wavelengths because these signals are preferentially amplified in the first stage of this dual-stage DRA, while the NF is higher at longer wavelengths, because these are preferentially amplified in the second stage. Recently, a similarly designed wideband DRA using a relatively short total length of highly nonlinear fiber based on 5 pumps and supporting 80 nm bandwidth in the C+L band was demonstrated with record gain of $\approx$27 dB and NF no worse than $\approx$5.8 dB [139]. Note, a dual-stage configuration enabled the additional design freedom to use different Raman gain fibers in the two sections, thereby allowing further improvements in DRA NF [140] and reduction in nonlinear noise penalties [141]. The theoretical analysis and a preliminary experimental investigation of the accumulation of nonlinear noise in cascaded DRAs and its effect on system reach has been reported recently [142], while the performance of a multi-span transmission link with a 75 nm broadband DRA over the C+L band has also been studied by using multiple DP-x-QAM signals [143].

Current trends for bandwidth expansion beyond the C-band are showing growing interest in backward Raman amplification for commercial deployments. When used as complementary to other amplification techniques (i.e. EDFA, SOA), Raman amplification remains a strong candidate for providing inline optical amplification that targets the expansion in bandwidth to take the most benefit from the already deployed fiber infrastructure.

C. Ultra-wideband Semiconductor Optical Amplifiers

Although much less mature with respect to the aforementioned solutions for optical amplification, SOAs have great potentials regarding compactness, cost-effectiveness and power-efficiency. By taking advantage of the III–V semiconductors

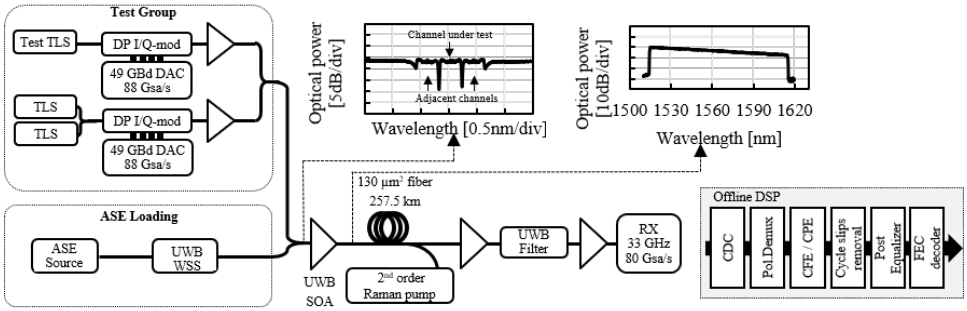

Figure 11: Experimental setup used in an unrepeated transmission over 100 nm bandwidth leveraging SOA and backward-Raman amplification [131].

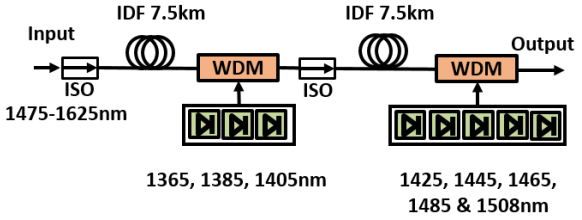

Figure 12: Schematic diagram of a dual-stage discrete S+C+L band Raman amplifier

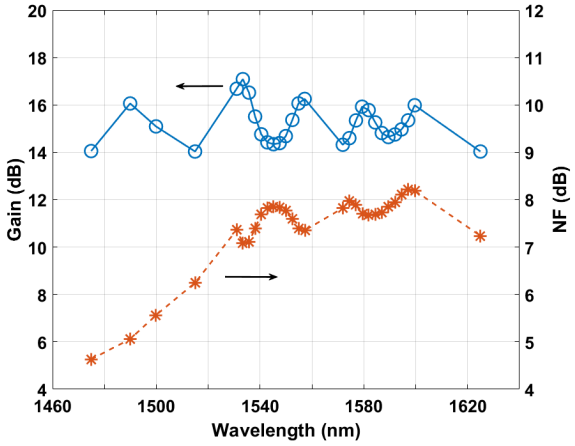

Figure 13: Measured gain and NF of dual-stage S+C+L band DRA..

manufacturing technology, SOAs can be monolithically integrated with lasers, modulators, or photodetectors to create added-value PICs with complex functionalities. By leveraging those properties, SOAs have been extensively investigated in the scientific community for the past decades as promising solutions for optical communications addressing various applications such as intensity noise suppression, fast optical switching, logical gates, optical regeneration and wavelength conversion [144]–[149]. Another flavor of SOAs is that their gain spectrum can be tailored to address virtually any relevant wavelength for optical communications through suitable material design and semiconductor bandgap engineering. SOA dimensions typically range from sub-millimeter to a few-millimeter long waveguide integrated devices providing lumped gain, thus able to compensate for fiber or lumped losses. However, their use in optical networks has traditionally been limited by their higher NF regarding EDFA, polarization dependent gain, as well as nonlinear dynamics occurring in the amplifiers upon saturation. This paradigm may now be shifted as recent advances in the SOA design and packaging have allowed to bridge the gap with fiber amplifiers. UWB-SOAs, in particular, are regarded as promising devices to extend the capacity of existing communication systems with custom designed SOAs demonstrated to exhibit more than 13 THz operational bandwidth, $\sim 3\times$ wider than standards C-band EDFAs.

In this section, we aim at summarizing such key technologies. Several research teams have reported SOA chips exhibiting a bandwidth larger than 100 nm [150]–[152] mainly based on Multi-Quantum Well (MQW) active layer, but none of them has achieved at the same time a high gain, a high saturation output power and a low NF. Another approach based on quantum dots (QD) active layer has led to wideband SOAs with a high saturation output power ($>$19 dBm) reaching a 3 dB bandwidth around 70 nm [153]. Based on MQW SOAs, 100+ nm UWB optical amplifiers tailored for WDM transmission systems have been recently developed [154] enabling the transport of total throughput $>$100 Tb/s. To the best of our knowledge, such a throughput is at least two orders of magnitude higher than the previously reported ones using SOA based repeaters [155]–[157].

UWB gain material relied on the unique ~~pioneering~~ approach demonstrated in [154], with InGaAsP MQW design tailored to maximize the energy spacing between the electronic transitions to extend the amplification bandwidth to more than 100 nm, as well as to increase the flat gain current to provide the largest gain – targeting $>$20 dB for small signals – and the lowest NF – reducing the gap with typical values of EDFAs of 4.5 dB. The developed UWB amplifiers exhibit optical gain over a spectral window wider than 100 nm, typically ranging from 1510 nm to 1620 nm as depicted by the Amplified Spontaneous Noise (ASE) spectrum in Fig. 14-a). Fig. 14-b) shows the measured characteristics of such UWB-SOA in terms of optical gain and NF versus wavelength. The 100+ nm wide amplifier exhibited an optical gain of 17 dB and a NF as low as 5.5 dB corresponding to the best reported values in the literature for SOAs [158]–[160]. This UWB amplifier has also been shown to provide more than 20 dBm output power when

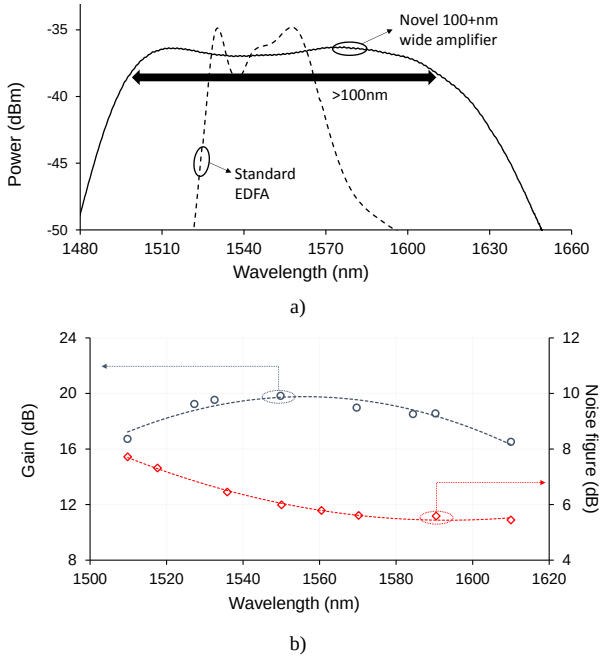

Figure 14: **a)** Comparison of amplified spontaneous emission noise spectrum of UWB amplifier with that of a C-band EDFA; **b)** gain (left) and NF (right) characteristics versus wavelength of 100+ nm UWB-SOA.

0 dBm optical power or more is injected at its input. Although further improvements in terms of output power and noise figure may be desirable through SOA design optimization, such characteristics already match the requirements of deployed WDM systems [161]. Relying upon a detailed theory of nonlinear propagation in SOA-amplified WDM systems based on time-domain first-order regular perturbation to rigorously account for both SOA and fiber induced nonlinear impairments – while transmitting advanced modulation formats for coherent WDM transmission [162] – investigations demonstrate that the nonlinear gain dynamics of tailored SOAs is not a hurdle to the deployment of the UWB-SOA device in dense WDM applications [163].

These ~~remarkable~~ results have been obtained by developing ~~an innovative~~ a polarization diversity architecture combining free space optics and semiconductor technologies, which alleviates the need for polarization alignment of the input signal into the amplifier and makes the SOA-based device compliant with WDM systems requirements. The polarization diversity architecture avoids the need for developing polarization insensitive SOA chips with UWB gain medium, in which the active region must be capable of amplifying simultaneously both Transverse Electric (TE) and Transverse Magnetic (TM) modes of the input light, resulting in complex design and significant impairments such as high coupling losses and polarization dependent gain [164] . The use of polarization diversity architecture was first reported in [165] based on a single SOA chip inside a loop architecture. The unique architecture reported in [154] embeds two singularly polarized SOAs in a parallel architecture, one for each polarization of the light with a single pass as described in Fig. 15-a). Free space optics is used to handle beam light splitting, coupling and polarization rotations between TE and TM modes. ~~The input light from the fiber is first split into TE and TM polarization modes using a birefringent material. The TM mode is then passed through a waveplate and rotated to the TE mode. Therefore,~~ The beam light on each optical path at the input of the SOA is aligned on TE mode. This enables the use of two optimized SOAs for TE polarization only, which greatly relaxes the constraint on the active layer section. Buried ridge SOAs have been fabricated with compressively strained quantum wells, especially designed to achieve significant large gain bandwidth. The stripes are tilted to reduce facet reflection, and these facets have been anti-reflection coated. Light coupling at input and output of the SOAs is obtained with micro-lenses. ~~Finally, the light on the first path is passed through a waveplate and rotated to the TM mode before being recombined with the TE mode of the second path by another birefringent material.~~ Each SOA can be driven independently, and a sensor was inserted in between the SOAs for thermal cooling. Although not reported on the schematic of Fig. 15-a), optical isolation realized in free space optics has also been added on input and output paths of the proposed amplifier modules. The inset of Fig. 15-a) shows the picture of the package module embedding the polarization diversity structure and a Peltier thermoelectric cooler.

Combining these novel extended-bandwidth SOA modules with the most recent advances in DSP and powerful flexible rate approaches (modulation formats and FEC coding), coherent WDM systems with seamless 100+ nm optical bandwidth have been demonstrated for the first time, reaching net throughputs >100 Tb/s [166], [167] as illustrated in Fig. 15-b). ~~illustrates this remarkable result by showing the measured per channel bit rates over this pioneering 100+ nm seamless optical bandwidth experiment.~~ Moreover, a field trial was conducted over Facebook facilities in the Paris area [168] with successful transport of real-time traffic at 250 Gb/s per wavelength, paving the way for future optical communications using SOA technologies.

Although the potential of UWB-SOA has only been demonstrated on the C- and L-bands to date to compete with available C + L-bands systems, tailored bandgap engineering would allow to reproduce such UWB-SOA devices to address any other transmission bands [169]. The use of UWB-SOA to address O-band or S-band to complement the traditional C+L-band systems towards multi-band systems applications appears attractive for scaling capacity of optical systems in the future. As it will be discussed in Sec. IV, this property could be also combined with a new type of UWB fibers.

IV. Next-generation UWB optical fibers

The simplest and most viable approach to exploit the throughput enhancement potential of the broadband devices discussed above is to use them in conjunction with conventional optical fibers. It is well known, in these glass core fibers the minimum attenuation is achieved in the C-band as reported in Fig. 1 and in Fig. 16-b). This falls at the intersection between the Rayleigh scattering curve (proportional to λ^{-4}) and the steep infrared multi-photon absorption curve ($C \cdot e^{-D/\lambda}$)

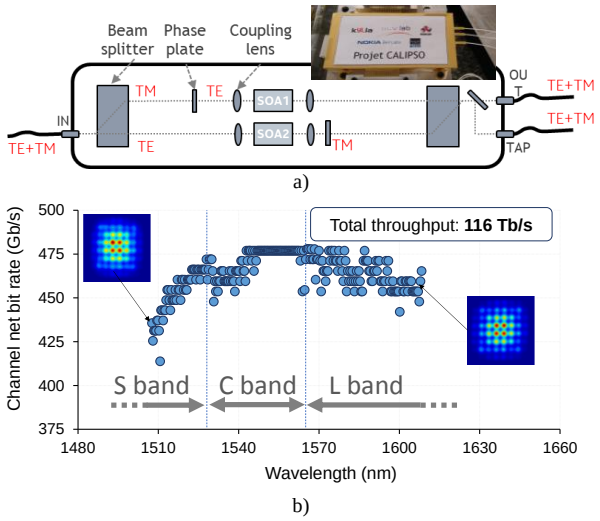

Figure 15: **a)** Schematic description of the polarization diversity architecture developed for UWB-SOAs, with the image of the realized packaged module in the inset; **b)** Measured net channel bit rates after 100 km transmission with adaptive constellation shaping, yielding a total throughput of 116 Tb/s over seamless 100+ nm optical bandwidth [166].

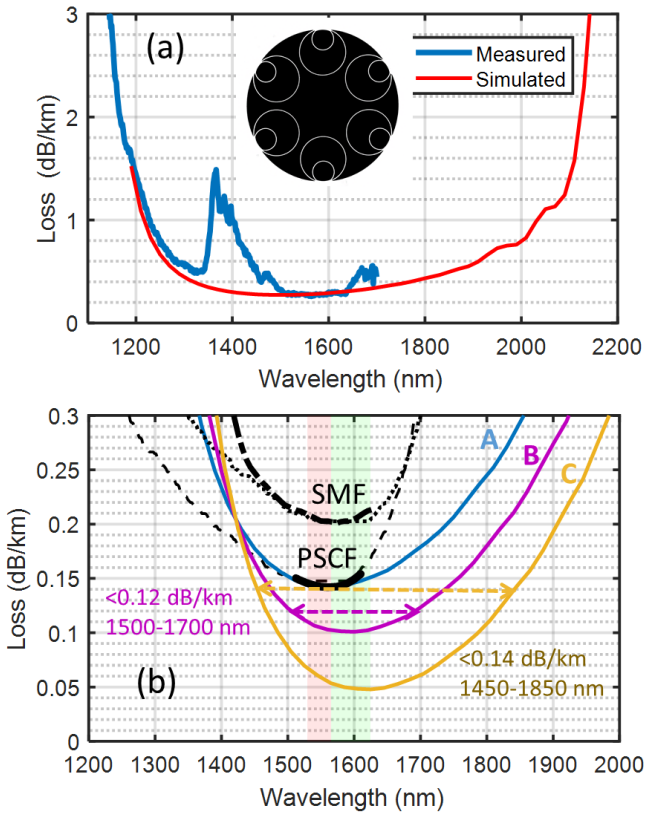

Figure 16: **(a)** Measured and simulated loss for a 0.28 dB/km NANF [171]; **(b)** Optical bandwidth prediction of what future NANFs might offer, obtained by simple down-scaling and spectral shifting of the simulated curve in **(a)**. Three cases illustrate scenarios where the minimum loss reaches 0.145 dB/km (A), 0.1 dB/km (B) and 0.05 dB/km (C). For comparison, the loss of standard SMF and of the lowest loss PSCF [178] are also shown.

of the silica glass [170]. These fundamental loss mechanisms are intrinsic for silica (doped or undoped) and produce the classical V-shaped attenuation curve, shown in Fig. 1 and Fig. 16-b) for SMF-28 and for Pure Silica Core Fiber (PSCF). This determines the operational bandwidth of standard fibers, which cannot be modified.

A potential solution to achieve fibers with an adequate loss for long distance optical communications over a broader bandwidth than SMF can offer, might come from HCF. In HCFs, light can be guided almost entirely in an air core, with an overlap with the surrounding glass that can be as little as 30–50 ppm. As a result, the spectral shape of their loss is not determined by the Rayleigh scattering or infrared multi-phonon absorption of the glass, but rather by a combination of leakage, surface scattering and micro/macro bend phenomena [171]. Consequently, HCFs offer, in principle, the potential for wider and flatter regions of minimum loss than SMF.

Loss in these fibers has gone through a rapid reduction in recent years: from 175 dB/km in 2015 [172] to 1.3 dB/km in 2018 [173], to 0.22 dB/km in 2021 [174] and, recently, down to 0.174 dB/km [175]). This brings us to speculate in this section what HCFs might offer for wide bandwidth optical communications if such a loss reduction trend continues. We will focus on a particular type of hollow core fiber, the NANF [176], which currently holds the above-mentioned record 0.174 dB/km for the lowest loss reported to date in an HCF and which has already shown the capability to transmit WDM data over >4000 km [177].

Speculating about the level of loss and bandwidth that might be offered by NANFs in the future is not an easy task, due to the subtle interplay of various loss mechanisms (leakage, surface scattering, microbend), each with its own spectral dependence. The simple approximated approach we have taken in this work to predict – to a first approximation – what might be the available bandwidth in future NANFs is explained in Fig. 16.

Fig. 16-a) plots the measured loss (up to the 1700 nm limit of the available Optical Spectrum Analyzer (OSA)) of a 0.28 dB/km NANF [171]. The figure also shows the excellent comparison with the simulated loss curve of the same fiber, obtained by modeling the leakage of its fabricated cross-section and by adding to it its estimated surface scattering (almost negligible) and microbend contributions [171]. As it can be seen, the loss presents a characteristic U-shape, determined by coupling with resonant glass tube modes at short wavelengths (1100 nm) and by leakage loss at long wavelengths (2100 nm). In Fig. 16-b) we assumed that through improvements in structure and fabrication process such a loss level can be reduced, but that its spectral shape remains unchanged. For illustration, we plot three curves where the simulated loss curve in Fig. 16-a) has been rigidly down-scaled to a minimum value of 0.145, 0.1 and 0.05 dB/km (curves (A), (B) and (C), respectively). A small spectral shift, easily achievable during fabrication with controllable modifications in the tube membrane thickness, was also applied. For comparison, we also plot the loss of a standard germanium doped SMF, and of the record low-loss PSCF.

The curve (A) shows that if NANF achieved the same minimum C-band loss as current PSCF (0.145 dB/km [178]),

the bandwidth offered by the HCF would be wider. For example, PSCF offers about 180 nm of spectrum with loss below 0.17 dB/km (1450–1630 nm), whereas NANF would offer 230 nm (1450–1680 nm). If the NANF minimum loss could be reduced down to 0.1 dB/km, curve (B) shows that a 200 nm bandwidth, from 1500 to 1700 nm would in principle be possible at a loss below 0.12 dB/km. Finally, curve (C) shows that in a NANF with a minimum loss of only 0.05 dB/km, propagation below 0.14 dB/km would be possible over as much as 400 nm, from 1450 to 1850 nm.

Clearly, these are only illustrative examples based on a hypothetical speculation; considerable more research and some inventive steps are required to produce fibers with such characteristics. This simple study, however, shows that a potential route to low-loss fibers with a broader bandwidth than current technology exists, at least in theory. Among the numerous engineering challenges that need to be overcome for such wide bandwidth fiber technology to become available, it is also worth mentioning the need for an improved control of the gas content inside the fibers. Like in free space optical communications, roto-vibrational absorption lines from gases such as H_2O, CO_2 or HCl can increase the propagation loss at specific wavelengths. One example of this is shown by the water vapor peak around 1400 nm (where the individual lines are unresolved by the large OSA bandwidth) that can be seen in Fig. 16-a). Although challenging, we believe that improved purification of gases and preforms during fabrication is a feasible strategy, which can mitigate the problem and open up large operational bandwidths.

One of the most attractive features of NANF for the purpose of data transmission is their *intrinsically low nonlinearity*. Although this has not yet been measured accurately for state-of-the-art NANFs, by combining the small glass overlap (which can be as small as 0.003%) with the Kerr nonlinearity of typical gases ($\sim$ 3 orders of magnitude lower than silica), and taking into account the larger effective area of NANF (with a Mode-Field Diameter (MFD), of 22-25 μm vs. 10-12 μm of glass-guiding fibers), nonlinear coefficients on the order of $\gamma = 10^{-4}$ to 10^{-3} (W km)$^{-1}$ are predicted. This is three to four orders of magnitude lower than in SMF.

Another aspect of relevance in relation to the possible use of NANF in high-performance long-haul transmission systems is Inter-Modal Interference (IMI). IMI occurs in NANFs because they are intrinsically multimodal. Although they can achieve effective single-mode operation by inducing large loss in all modes except the fundamental one, IMI can still be significant if the higher-mode suppression mechanism is not strong enough. However, substantial progress has been obtained recently in IMI suppression as well (see further below).

Given the recent progress in all aspects related to NANF performance, these fibers have been recently used to perform long-haul WDM transmission experiments. Progress has been substantial over the last few years, paralleling that of the fiber performance. Polarization Division Multiplexing - Quadrature Phase Shift Keying (PDM - QPSK) transmission at 32 GBaud reached 341 km [179] in 2019, 618 km [180] in 2020 and more than 4,000 km [177] in 2021. These experiments were performed in recirculating loops, where the NANF section had length of 4.8, 7.7 and 11.5 km, respectively. Most of the progress seen in these experiments has been attributed to improving IMI performance, estimated at -35 dB/km in [180] and -45 to -55 dB/km in [177].

The possible throughput potential of NANF has been recently investigated in [181], where hypothetical scenarios arising from future high-performance NANF are explored. The paper shows that ultra-wide-band transmission over NANF holds the promise for a substantial potential increase of throughput vs. traditional solid-core fibers. To realize such potential, [181] argues that significant technological challenges need to be overcome besides improving NANF, such as (among many) the need for unconventional-band amplification technologies, transmission at high bits/symbol, management of large launched power, splicing, cabling and muxing technologies. However, the rapid pace of progress of the last few years in NANF performance may provide incentives towards developing such supporting technologies, in view of the considerable throughput increase that NANF could potentially grant.

V. Conclusions

Devices designed for ultra-wideband operation beyond the C- and L-bands are key enabling technologies for increasing capacity in future generation optical transmission systems. In this review paper, we outline the state-of-the-art of tunable lasers, amplifiers, optical switches, modulators and the recently introduced hollow-core nested antiresonant nodeless fibers (NANFs). While NANFs deal with long term evolution of optical networks, the research efforts and progress at pace on UWB tunable lasers, modulators, amplifiers and optical switches open up the development of UWB systems with adequate combinations of devices and components, depending on the envisioned scenarios, e.g., metro/access, long-haul and ultra-long-haul. The path toward bandwidth extension of existing optical systems in the S-, O-, E-bands, and possibly others, requires ultra-wideband technologies achieving simultaneously performance inline with WDM systems requirements and low-cost targets, and the challenges to address these requirements have been discussed for the future generation ultra-wideband transmission devices and fibers, including component integration, fabrication, new materials. The merits and challenges of UWB optical transport systems to meet WDM system requirements are presented extensively in a companion paper in this special issue [182], focusing on the unique technical issues to UWB systems including modeling, design, and impairments mitigation. While the throughput of conventional systems is getting saturated, these papers show that several innovative technologies exist that provide a credible path towards the much increased transmission capability that the fast-growing traffic demand will unavoidably require in the years to come.

References

[1] "Cisco Annual Internet Report (2018–2023) White Paper," Link to the document.

[2] C. R. Fludger, T. Duthel, D. Van den Borne, C. Schulien, E. D. Schmidt, T. Wuth, J. Geyer, E. De Man, G.-D. Khoe, and H. de Waardt, "Coherent equalization and POLMUX-RZ-DQPSK for robust 100-GE transmission," *Journal of Lightwave Technology*, vol. 26, no. 1, pp. 64–72, 2008.

[3] G. Charlet, J. Renaudier, H. Mardoyan, P. Tran, O. Bertran-Pardo, F. Verluise, M. Achouche, A. Boutin, F. Blache, J.-Y. Dupuy, and S. Bigo, "Transmission of 16.4-Tbit/s capacity over 2550 km using PDM-QPSK modulation format and coherent receiver," *Journal of Lightwave Technology*, vol. 27, no. 3, pp. 153–157, 2009.

[4] H. Sun, M. Torbatian, M. Karimi, R. Maher, S. Thomson, M. Tehrani, Y. Gao, A. Kumpera, G. Soliman, A. Kakkar *et al.*, "800G DSP ASIC design using probabilistic shaping and digital sub-carrier multiplexing," *Journal of Lightwave Technology*, vol. 38, no. 17, pp. 4744–4756, 2020.

[5] J. Renaudier, R. Rios-Müller, P. Tran, L. Schmalen, and G. Charlet, "Spectrally efficient 1-Tb/s transceivers for long-haul optical systems," *Journal of Lightwave Technology*, vol. 33, no. 7, pp. 1452–1458, 2015.

[6] R. Gallager, "Low-density parity-check codes," *IRE Transactions on information theory*, vol. 8, no. 1, pp. 21–28, 1962.

[7] M. Arabaci, I. B. Djordjevic, R. Saunders, and R. M. Marcoccia, "High-rate nonbinary regular quasi-cyclic LDPC codes for optical communications," *Journal of Lightwave Technology*, vol. 27, no. 23, pp. 5261–5267, 2009.

[8] K. Sugihara, Y. Miyata, T. Sugihara, K. Kubo, H. Yoshida, W. Matsumoto, and T. Mizuochi, "A spatially-coupled type LDPC code with an NCG of 12 dB for optical transmission beyond 100 Gb/s," in *Optical Fiber Communication Conference*. Optical Society of America, 2013, pp. OM2B–4.

[9] E. Ip and J. M. Kahn, "Compensation of dispersion and nonlinear impairments using digital backpropagation," *Journal of Lightwave Technology*, vol. 26, no. 20, pp. 3416–3425, 2008.

[10] F. P. Guiomar and A. N. Pinto, "Simplified Volterra series nonlinear equalizer for polarization-multiplexed coherent optical systems," *Journal of Lightwave Technology*, vol. 31, no. 23, pp. 3879–3891, 2013.

[11] F. Buchali, G. Böcherer, W. Idler, L. Schmalen, P. Schulte, and F. Steiner, "Experimental demonstration of capacity increase and rate-adaptation by probabilistically shaped 64-QAM," in *2015 European Conference on Optical Communication (ECOC)*. IEEE, 2015, pp. 1–3.

[12] G. Böcherer, F. Steiner, and P. Schulte, "Bandwidth efficient and rate-matched low-density parity-check coded modulation," *IEEE Transactions on communications*, vol. 63, no. 12, pp. 4651–4665, 2015.

[13] G. Kramer, M. I. Yousefi, and F. R. Kschischang, "Upper bound on the capacity of a cascade of nonlinear and noisy channels," in *2015 IEEE Information Theory Workshop (ITW)*. IEEE, 2015, pp. 1–4.

[14] A. Napoli, Z. Maalej, V. A. Sleiffer, M. Kuschnerov, D. Rafique, E. Timmers, B. Spinnler, T. Rahman, L. D. Coelho, and N. Hanik, "Reduced complexity digital back-propagation methods for optical communication systems," *Journal of Lightwave Technology*, vol. 32, no. 7, pp. 1351–1362, 2014.

[15] M. Salsi, C. Koebele, D. Sperti, P. Tran, H. Mardoyan, P. Brindel, S. Bigo, A. Boutin, F. Verluise, P. Sillard, M. Astruc, L. Provost, and G. Charlet, "Mode-division multiplexing of 2 $\times$100 Gb/s channels using an LCOS-based spatial modulator," *Journal of Lightwave Technology*, vol. 30, no. 4, pp. 618–623, 2012.

[16] S. Beppu, K. Igarashi, M. Kikuta, D. Soma, T. Nagai, Y. Saito, H. Takahashi, T. Tsuritani, I. Morita, and M. Suzuki, "Weakly coupled 10-mode-division multiplexed transmission over 48-km few-mode fibers with real-time coherent mimo receivers," *Opt. Express*, vol. 28, no. 13, pp. 19 655–19 668, Jun 2020. [Online]. Available: http://opg.optica.org/oe/abstract.cfm?URI=oe-28-13-19655

[17] S. Randel, R. Ryf, A. Sierra, P. J. Winzer, A. H. Gnauck, C. A. Bolle, R.-J. Essiambre, D. W. Peckham, A. McCurdy, and R. Lingle, "6×56-Gb/s mode-division multiplexed transmission over 33-km few-mode fiber enabled by 6×6 MIMO equalization," *Opt. Express*, vol. 19, no. 17, pp. 16 697–16 707, Aug 2011. [Online]. Available: http://opg.optica.org/oe/abstract.cfm?URI=oe-19-17-16697

[18] K. Igarashi, T. Tsuritani, I. Morita, Y. Tsuchida, K. Maeda, M. Tadakuma, T. Saito, K. Watanabe, K. Imamura, R. Sugizaki *et al.*, "1.03-Exabit/skm super-Nyquist-WDM transmission over 7,326-km seven-core fiber," in *39th European Conference and Exhibition on Optical Communication (ECOC 2013)*. IET, 2013, pp. 1–3.

[19] A. Turukhin, O. V. Sinkin, H. Batshon, H. Zhang, Y. Sun, M. Mazurczyk, C. R. Davidson, J.-X. Cai, M. A. Bolshtyansky, D. G. Foursa *et al.*, "105.1 Tb/s power-efficient transmission over 14,350 km using a 12-core fiber," in *2016 Optical Fiber Communications Conference and Exhibition (OFC)*. IEEE, 2016, pp. 1–3.

[20] A. Turukhin, H. Batshon, M. Mazurczyk, Y. Sun, C. Davidson, J.-X. Chai, O. Sinkin, W. Patterson, G. Wolter, M. Bolshtyansky *et al.*, "Demonstration of 0.52 Pb/s potential transmission capacity over 8,830 km using multicore fiber," in *ECOC 2016; 42nd European Conference on Optical Communication*. VDE, 2016, pp. 1–3.

[21] M. Cantono, D. Pilori, A. Ferrari, C. Catanese, J. Thouras, J.-L. Augé, and V. Curri, "On the interplay of nonlinear interference generation with stimulated Raman scattering for QoT estimation," *Journal of Lightwave Technology*, vol. 36, no. 15, pp. 3131–3141, 2018.

[22] A. Ferrari, A. Napoli, J. K. Fischer, N. Costa, A. D'Amico, J. Pedro, W. Forysiak, E. Pincemin, A. Lord, A. Stavdas *et al.*, "Assessment on the achievable throughput of multi-band ITU-T G. 652. D fiber transmission systems," *Journal of Lightwave Technology*, vol. 38, no. 16, pp. 4279–4291, 2020.

[23] D. Semrau, R. I. Killey, and P. Bayvel, "The Gaussian noise model in the presence of inter-channel stimulated Raman scattering," *Journal of Lightwave Technology*, vol. 36, no. 14, pp. 3046–3055, 2018.

[24] A. Ferrari, A. Napoli, J. K. Fischer, N. Costa, J. Pedro, N. Sambo, E. Pincemin, B. Sommerkohrn-Krombholz, and V. Curri, "Upgrade capacity scenarios enabled by multi-band optical systems," in *2019 21st International Conference on Transparent Optical Networks (ICTON)*. IEEE, 2019, pp. 1–4.

[25] E. Dianov, S. Firstov, S. Alyshev, A. Kharakhordin, K. Riumkin, M. Melkumov, V. Khopin, and A. Guryanov, "Bismuth-doped optical fibers for the telecommunication L and U bands: Effect of laser and thermal treatment on gain characteristics," in *2018 European Conference on Optical Communication (ECOC)*. IEEE, 2018, pp. 1–3.

[26] "Handbook – Optical fibres, cables and systems - ITU, 2009," https://www.itu.int/dms_pub/itu-t/opb/hdb/T-HDB-OUT.10-2009-1-PDF-E.pdf.

[27] H. Hu and L. K. Oxenløwe, "Chip-based optical frequency combs for high-capacity optical communications," *Nanophotonics*, vol. 10, no. 5, pp. 1367–1385, 2021.

[28] H. Debrégeas, *Widely Tunable Laser Diodes*. Cham: Springer International Publishing, 2017, pp. 209–248.

[29] H. Hatakeyama, K. Kudo, Y. Yokoyama, K. Naniwae, and T. Sasaki, "Wavelength-selectable microarray light sources for wide-band DWDM applications," *IEEE Journal of Selected Topics in Quantum Electronics*, vol. 8, no. 6, pp. 1341–1348, 2002.

[30] H. Ishii, K. Kasaya, H. Oohashi, Y. Shibata, H. Yasaka, and K. Okamoto, "Widely wavelength-tunable DFB laser array integrated with funnel combiner," *IEEE Journal of Selected Topics in Quantum Electronics*, vol. 13, no. 5, pp. 1089–1094, 2007.

[31] B. Pezeshki, E. Vail, J. Kubicky, G. Yoffe, S. Zou, J. Heanue, P. Epp, S. Rishton, D. Ton, B. Faraji, M. Emanuel, X. Hong, M. Sherback, V. Agrawal, C. Chipman, and T. Razazan, "20-mw widely tunable laser module using DFB array and MEMS selection," *IEEE Photonics Technology Letters*, vol. 14, no. 10, pp. 1457–1459, 2002.

[32] H. Debrégeas-Sillard, C. Fortin, F. Pommereau, D. Drugeon, Y. Gottesman, O. Drisse, E. Derouin, B. Rousseau, N. Lagay, F. Martin, J. Landreau, and C. Kazmierski, "More than 40nm tuning DBR-MMI-SOA with only one Bragg current control, compatible with fast switching," in *33rd European Conference and Exhibition of Optical Communication*, 2007, pp. 1–2.

[33] V. Jayaraman, Z.-M. Chuang, and L. Coldren, "Theory, design, and performance of extended tuning range semiconductor lasers with sampled gratings," *IEEE Journal of Quantum Electronics*, vol. 29, no. 6, pp. 1824–1834, 1993.

[34] H. Ishii, H. Tanobe, F. Kano, Y. Tohmori, Y. Kondo, and Y. Yoshikuni, "Quasicontinuous wavelength tuning in super-structure-grating (SSG) DBR lasers," *IEEE Journal of Quantum Electronics*, vol. 32, no. 3, pp. 433–441, 1996.

[35] M. A. Tran, D. Huang, and J. E. Bowers, "Tutorial on narrow linewidth tunable semiconductor lasers using Si/III-V heterogeneous integration," *APL Photonics*, vol. 4, no. 11, p. 111101, 2019.

[36] K. Takabayashi, K. Takada, N. Hashimoto, M. Doi, S. Tomabechi, T. Nakazawa, and K. Morito, "Widely (132 nm) wavelength tunable laser using a semiconductor optical amplifier and an acousto-optic tunable filter," *Electronics Letters*, vol. 40, pp. 1187 – 1188, 10 2004.

[37] C. Calò, K. Benyahya, H. Mardoyan, P. Charbonnier, D. Sacchetto, M. Zervas, K. Mekhazni, D. Lanteri, H. Gariah, C. Fortin *et al.*, "Hybrid InP-SiN microring-resonator based tunable laser with high output power and narrow linewidth for high capacity coherent systems," in *2022 Optical Fiber Communications Conference and Exhibition (OFC)*, 2022, pp. 1–3.

[38] H. Yamazaki, M. Takahashi, K. Suzuki, Y. Deki, T. Takeuchi, S. Takaesu, M. Horie, K. Sato, and K. Kudo, "A widely tunable laser using silica-waveguide ring resonators," in *Active and Passive Optical Components for WDM Communications V*, A. K. Dutta, Y. Ohishi, N. K. Dutta, and J. Moerk, Eds., vol. 6014, International Society for Optics and Photonics. SPIE, 2005, pp. 50 – 58. [Online]. Available: https://doi.org/10.1117/12.630146

[39] T. Takeuchi, M. Takahashi, K. Suzuki, S. Watanabe, and H. Yamazaki, "Wavelength Tunable Laser with Silica-Waveguide Ring Resonators," *IEICE Transactions on Electronics*, vol. 92, no. 2, pp. 198–204, Jan. 2009.

[40] A. Verdier, G. de Valicourt, R. Brenot, H. Debregeas, P. Dong, M. Earnshaw, H. CarrËre, and Y.-K. Chen, "Ultrawideband wavelength-tunable hybrid external-cavity lasers," *Journal of Lightwave Technology*, vol. 36, no. 1, pp. 37–43, 2018.

[41] K.-J. Boller, A. van Rees, Y. Fan, J. Mak, R. Lammerink, C. Franken, P. van der Slot, D. Marpaung, C. Fallnich, J. Epping, R. Oldenbeuving, D. Geskus, R. Dekker, I. Visscher, R. Grootjans, C. Roeloffzen, M. Hoekman, E. Klein, A. Leinse, and R. Heideman, "Hybrid integrated semiconductor lasers with silicon nitride feedback circuits," *Photonics*, vol. 7, no. 1, 2020.

[42] H. Guan, A. Novack, T. Galfsky, Y. Ma, S. Fathololoumi, A. Horth, T. N. Huynh, J. Roman, R. Shi, M. Caverley, Y. Liu, T. Baehr-Jones, K. Bergman, and M. Hochberg, "Widely-tunable, narrow-linewidth III-V/Silicon hybrid external-cavity laser for coherent communication," *Opt. Express*, vol. 26, no. 7, pp. 7920–7933, Apr 2018. [Online]. Available: http://www.opticsexpress.org/abstract.cfm?URI=oe-26-7-7920

[43] M. Theurer, M. Moehrle, A. Sigmund, K.-O. Velthaus, R. M. Oldenbeuving, L. Wevers, F. M. Postma, R. Mateman, F. Schreuder, D. Geskus, K. Wˆrhoff, R. Dekker, R. G. Heideman, and M. Schell, "Flip-chip integration of InP to SiN photonic integrated circuits," *Journal of Lightwave Technology*, vol. 38, no. 9, pp. 2630–2636, 2020.

[44] T. Komljenovic, L. Liang, R.-L. Chao, J. Hulme, S. Srinivasan, M. Davenport, and J. E. Bowers, "Widely-tunable ring-resonator semiconductor lasers," *Applied Sciences*, vol. 7, no. 7, 2017. [Online]. Available: https://www.mdpi.com/2076-3417/7/7/732

[45] J. Zhang, A. Gocalinkska, E. Pelucchi, J. Van Campenhout, G. Lepage, P. Verheyen, B. Corbett, and G. Roelkens, "III-V-on-Silicon widely tunable laser realized using micro-tranfer-printing," in *45th European Conference on Optical Communication (ECOC 2019)*, 2019, pp. 1–4.

[46] H. Elfaiki, K. Hassan, G.-H. Duan, C. Jany, S. Malhouitre, T. Verolet, A. Gallet, C. Caillaud, A. Shen, D. Make, H. Gariah, V. Muffato, A. Coquiard, S. Olivier, H. Benisty, and M. Achouche, "Ultra wide hybrid III-V on silicon tunable laser," in *2018 European Conference on Optical Communication (ECOC)*, 2018, pp. 1–3.

[47] Fujitsu, https://www.fujitsu.com/jp/group/foc/en/products/devices/indexgig5.html.

[48] EOSpace, "40+gb/s modulators," https://www.eospace.com/product-summary-modulator.

[49] Thorlabs, "Lithium niobate electro-optic modulators, fiber-coupled," https://www.thorlabs.com/.

[50] P. C. Schindler, D. Korn, C. Stamatiadis, M. F. O'Keefe, L. Stampoulidis, R. Schmogrow, P. Zakynthinos, R. Palmer, N. Cameron, Y. Zhou, R. G. Walker, E. Kehayas, S. Ben-Ezra, I. Tomkos, L. Zimmermann, K. Petermann, W. Freude, C. Koos, and J. Leuthold, "Monolithic GaAs electro-optic IQ modulator demonstrated at 150 Gbit/s with 64QAM," *Journal of Lightwave Technology*, vol. 32, no. 4, pp. 760–765, 2014.

[51] Y. Ogiso, J. Ozaki, Y. Ueda, H. Wakita, M. Nagatani, H. Yamazaki, M. Nakamura, T. Kobayashi, S. Kanazawa, Y. Hashizume, H. Tanobe, N. Nunoya, M. Ida, Y. Miyamoto, and M. Ishikawa, "80-GHz bandwidth and 1.5-V vπ InP-Based IQ modulator," *Journal of Lightwave Technology*, vol. 38, no. 2, pp. 249–255, 2020.

[52] R. A. Griffin, S. K. Jones, N. Whitbread, S. C. Heck, and L. N. Langley, "InP Mach–Zehnder modulator platform for 10/40/100/200-Gb/s operation," *IEEE Journal of Selected Topics in Quantum Electronics*, vol. 19, no. 6, pp. 158–166, 2013.

[53] G. T. Reed, G. Mashanovich, F. Y. Gardes, and D. J. Thomson, "Silicon optical modulators," *Nature Photonics*, vol. 4, no. 518, 2010.

[54] K.-O. Velthaus, N. Wolf, J. H. Choi, L. Yan, P. Harati, M. Gruner, B. G. Saavedra, M. Rausch, H.-G. Bach, and M. Schell, "Impedance-engineered low power MZM / driver assembly for CFP4-size pluggable long haul and metro transceiver," in *2014 The European Conference on Optical Communication (ECOC)*, 2014, pp. 1–3.

[55] W. Heni, B. Baeuerle, H. Mardoyan, F. Jorge, J. M. Estaran, A. Konczykowska, M. Riet, B. Duval, V. Nodjiadjim, M. Goix, J.-Y. Dupuy, M. Destraz, C. Hoessbacher, Y. Fedoryshyn, H. Xu, D. L. Elder, L. R. Dalton, J. Renaudier, and J. Leuthold, "Ultra-high-speed 2:1 digital selector and plasmonic modulator IM/DD transmitter operating at 222 GBaud for intra-datacenter applications," *Journal of Lightwave Technology*, vol. 38, no. 9, pp. 2734–2739, 2020.

[56] B. Baeuerle, W. Heni, C. Hoessbacher, Y. Fedoryshyn, U. Koch, A. Josten, T. Watanabe, C. Uhl, H. Hettrich, D. L. Elder, L. R. Dalton, M. Möller, and J. Leuthold, "120 GBd plasmonic Mach-Zehnder modulator with a novel differential electrode design operated at a peak-to-peak drive voltage of 178 mv," *Opt. Express*, vol. 27, no. 12, pp. 16 823–16 832, Jun 2019. [Online]. Available: http://www.opticsexpress.org/abstract.cfm?URI=oe-27-12-16823

[57] M. Ayata, Y. Fedoryshyn, W. Heni, B. Baeuerle, A. Josten, M. Zahner, U. Koch, Y. Salamin, C. Hoessbacher, C. Haffner, D. L. Elder, L. R. Dalton, and J. Leuthold, "High-speed plasmonic modulator in a single metal layer," *Science*, vol. 358, no. 6363, pp. 630–632, 2017. [Online]. Available: https://science.sciencemag.org/content/358/6363/630

[58] S. Wolf, H. Zwickel, C. Kieninger, M. Lauermann, W. Hartmann, Y. Kutuvantavida, W. Freude, S. Randel, and C. Koos, "Coherent modulation up to 100 GBd 16QAM using silicon-organic hybrid (SOH) devices," *Opt. Express*, vol. 26, no. 1, pp. 220–232, Jan 2018. [Online]. Available: http://www.opticsexpress.org/abstract.cfm?URI=oe-26-1-220

[59] C. Kieninger, C. Füllner, H. Zwickel, Y. Kutuvantavida, J. N. Kemal, C. Eschenbaum, D. L. Elder, L. R. Dalton, W. Freude, S. Randel, and C. Koos, "Silicon-organic hybrid (SOH) Mach-Zehnder modulators for 100 GBd PAM4 signaling with sub-1-dB phase-shifter loss," *Opt. Express*, vol. 28, no. 17, pp. 24 693–24 707, Aug 2020. [Online]. Available: http://www.opticsexpress.org/abstract.cfm?URI=oe-28-17-24693

[60] H. Zwickel, J. N. Kemal, C. Kieninger, Y. Kutuvantavida, J. Rittershofer, M. Lauermann, W. Freude, S. Randel, and C. Koos, "Electrically packaged silicon-organic hybrid (SOH) I/Q-modulator for 64 GBd operation," *Opt. Express*, vol. 26, no. 26, pp. 34 580–34 591, Dec 2018. [Online]. Available: http://www.opticsexpress.org/abstract.cfm?URI=oe-26-26-34580

[61] A. J. Mercante, S. Shi, P. Yao, L. Xie, R. M. Weikle, and D. W. Prather, "Thin film lithium niobate electro-optic modulator with terahertz operating bandwidth," *Opt. Express*, vol. 26, no. 11, pp. 14 810–14 816, May 2018. [Online]. Available: http://www.opticsexpress.org/abstract.cfm?URI=oe-26-11-14810

[62] V. E. Stenger, J. Toney, A. PoNick, D. Brown, B. Griffin, R. Nelson, and S. Sriram, "Low loss and low Vpi thin film lithium niobate on quartz electro-optic modulators," in *2017 European Conference on Optical Communication (ECOC)*, 2017, pp. 1–3.

[63] C. Wang, M. Zhang, B. Stern, M. Lipson, and M. Lončar, "Nanophotonic lithium niobate electro-optic modulators," *Opt. Express*, vol. 26, no. 2, pp. 1547–1555, Jan 2018. [Online]. Available: http://www.opticsexpress.org/abstract.cfm?URI=oe-26-2-1547

[64] M. Zhang, C. Wang, P. Kharel, D. Zhu, and M. Lončar, "Integrated lithium niobate electro-optic modulators: when performance meets scalability," *Optica*, vol. 8, no. 5, pp. 652–667, May 2021. [Online]. Available: http://www.osapublishing.org/optica/abstract.cfm?URI=optica-8-5-652

[65] C. Wang, M. Zhang, X. Chen, M. Bertrand, A. Shams-Ansari, S. Chandrasekhar, P. Winzer, and M. Loncar, "Integrated lithium niobate electro-optic modulators operating at CMOS-compatible voltages," *Nature*, vol. 562, pp. 101–104, 2018.

[66] F. Eltes, C. Mai, D. Caimi, M. Kroh, Y. Popoff, G. Winzer, D. Petousi, S. Lischke, J. E. Ortmann, L. Czornomaz, L. Zimmermann, J. Fompeyrine, and S. Abel, "A BaTiO3-based electro-optic pockels modulator monolithically integrated on an advanced silicon photonics platform," *Journal of Lightwave Technology*, vol. 37, no. 5, pp. 1456–1462, 2019.

[67] P. Rabiei, J. Ma, S. Khan, J. Chiles, and S. Fathpour, "Heterogeneous lithium niobate photonics on silicon substrates," *Opt. Express*, vol. 21, no. 21, pp. 25 573–25 581, Oct 2013. [Online]. Available: http://www.opticsexpress.org/abstract.cfm?URI=oe-21-21-25573

[68] N. Boynton, H. Cai, M. Gehl, S. Arterburn, C. Dallo, A. Pomerene, A. Starbuck, D. Hood, D. C. Trotter, T. Friedmann, C. T. DeRose, and A. Lentine, "A heterogeneously integrated silicon photonic/lithium niobate travelling wave electro-optic modulator," *Opt. Express*, vol. 28, no. 2, pp. 1868–1884, Jan 2020. [Online]. Available: http://www.opticsexpress.org/abstract.cfm?URI=oe-28-2-1868

[69] A. N. R. Ahmed, S. Shi, A. Mercante, S. Nelan, P. Yao, and D. W. Prather, "High-efficiency lithium niobate modulator for K band operation," *APL Photonics*, vol. 5, no. 9, p. 091302, 2020.

[70] M. Xu, W. Chen, M. He, X. Wen, Z. Ruan, J. Xu, L. Chen, L. Liu, S. Yu, and X. Cai, "Michelson interferometer modulator based on

hybrid silicon and lithium niobate platform," *APL Photonics*, vol. 4, no. 10, p. 100802, 2019.

[71] M. Doi, M. Sugiyama, K. Tanaka, and M. Kawai, "Advanced LiNbO/sub 3/ optical modulators for broadband optical communications," *IEEE Journal of Selected Topics in Quantum Electronics*, vol. 12, no. 4, pp. 745–750, 2006.

[72] G.-W. Lu, J. Hong, F. Qiu, A. M. Spring, T. Kashino, J. Oshima, M.-a. Ozawa, H. Nawata, and S. Yokoyama, "High-temperature-resistant silicon-polymer hybrid modulator operating at up to 200 gbit s^{-1} for energy-efficient datacentres and harsh-environment applications," *Nature Communications*, vol. 11, no. 4224, 2020.

[73] S. Ummethalal, J. N. Kemal, M. Lauermann, A. Alam, H. Zwickel, T. Harter, Y. Kutuvantavida, L. Hahn, S. H. Nandam, D. L. Elder, L. R. Dalton, W. Freude, S. Randel, and C. Koos, "Capacitively coupled silicon-organic hybrid modulator for 200 Gbit/S PAM-4 signaling," in *2019 Conference on Lasers and Electro-Optics (CLEO)*, 2019, pp. 1–2.

[74] P. Bhasker, J. Norman, J. Bowers, and N. Dagli, "Low voltage, high optical power handling capable, bulk compound semiconductor electro-optic modulators at 1550 nm," *Journal of Lightwave Technology*, vol. 38, no. 8, 2020.

[75] J. H. Shin and N. Dagli, "Ultralow drive voltage substrate removed GaAs/AlGaAs electro-optic modulators at 1550 nm," *IEEE Journal of Selected Topics in Quantum Electronics*, vol. 19, no. 6, pp. 150–157, 2013.

[76] https://axenic.co.uk/.

[77] Y. Ogiso, J. Ozaki, Y. Ueda, N. Kashio, N. Kikuchi, E. Yamada, H. Tanobe, S. Kanazawa, H. Yamazaki, Y. Ohiso, T. Fujii, and M. Kohtoku, "Over 67 GHz bandwidth and 1.5 V vπ InP-based optical IQ modulator with n-i-p-n heterostructure," *Journal of Lightwave Technology*, vol. 35, no. 8, pp. 1450–1455, 2017.

[78] V. Lal, P. Studenkov, T. Frost, H. Tsai, B. Behnia, J. Osenbach, S. Wolf, R. Going, S. Porto, R. Maher, H. Hodaei, J. Zhang, C. Di Giovanni, K. Hoshino, T. Vallaitis, B. Ellis, J. Yan, K. Fong, E. Sooudi, M. Kuntz, S. Buggaveeti, D. Pavinski, S. Sanders, Z. Wang, G. Hoefler, P. Evans, S. Corzine, T. Butrie, M. Ziari, F. Kish, and D. Welch, "1.6Tbps coherent 2-channel transceiver using a monolithic Tx/Rx InP PIC and single SiGe ASIC," in *2020 Optical Fiber Communications Conference and Exhibition (OFC)*, 2020, pp. 1–3.

[79] P. O. Weigel, J. Zhao, K. Fang, H. Al-Rubaye, D. Trotter, D. Hood, J. Mudrick, C. Dallo, A. T. Pomerene, A. L. Starbuck, C. T. DeRose, A. L. Lentine, G. Rebeiz, and S. Mookherjea, "Bonded thin film lithium niobate modulator on a silicon photonics platform exceeding 100 ghz 3-db electrical modulation bandwidth," *Opt. Express*, vol. 26, no. 18, pp. 23 728–23 739, Sep 2018. [Online]. Available: http://www.opticsexpress.org/abstract.cfm?URI=oe-26-18-23728

[80] M. Xu, M. He, H. Zhang, J. Jian, Y. Pan, X. Liu, L. Chen, X. Meng, H. Chen, Z. Li, X. Xiao, S. Yu, S. Yu, and X. Cai, "High-performance coherent optical modulators based on thin-film lithium niobate platform," *Nature Communications*, vol. 11, no. 3911, 2020.

[81] V. Stenger, J. E. Toney, J. Scholl, J. Busch, A. Pollick, P. Pontius, and S. Sriram, "Wide-band electro-optic modulator in thin-film lithium niobate on quartz substrate," in *2012 38th European Conference and Exhibition on Optical Communications*, 2012, pp. 1–3.

[82] T. Ren, M. Zhang, C. Wang, L. Shao, C. Reimer, Y. Zhang, O. King, R. Esman, T. Cullen, and M. Lončar, "An integrated low-voltage broadband Lithium niobate phase modulator," *IEEE Photonics Technology Letters*, vol. 31, no. 11, pp. 889–892, 2019.

[83] J. Zhou, J. Wang, L. Zhu, Q. Zhang, and J. Hong, "Silicon photonics carrier depletion modulators capable of 85Gbaud 16QAM and 64Gbaud 64QAM," in *2019 Optical Fiber Communications Conference and Exhibition (OFC)*, 2019, pp. 1–3.

[84] J. Lin, H. Sepehrian, L. A. Rusch, and W. Shi, "Single-carrier 72 GBaud 32QAM and 84 GBaud 16QAM transmission using a SiP IQ modulator with joint digital-optical pre-compensation," *Opt. Express*, vol. 27, no. 4, pp. 5610–5619, Feb 2019. [Online]. Available: http://www.opticsexpress.org/abstract.cfm?URI=oe-27-4-5610

[85] D. J. Thomson, F. Y. Gardes, J.-M. Fedeli, S. Zlatanovic, Y. Hu, B. P. P. Kuo, E. Myslivets, N. Alic, S. Radic, G. Z. Mashanovich, and G. T. Reed, "50-Gb/s silicon optical modulator," *IEEE Photonics Technology Letters*, vol. 24, no. 4, pp. 234–236, 2012.

[86] M. Streshinsky, R. Ding, Y. Liu, A. Novack, Y. Yang, Y. Ma, X. Tu, E. K. S. Chee, A. E.-J. Lim, P. G.-Q. Lo, T. Baehr-Jones, and M. Hochberg, "Low power 50 Gb/s silicon traveling wave Mach-Zehnder modulator near 1300 nm," *Opt. Express*, vol. 21, no. 25, pp. 30 350–30 357, Dec 2013. [Online]. Available: http://www.opticsexpress.org/abstract.cfm?URI=oe-21-25-30350

[87] H. Xu, X.-Y. Li, X. Xiao, Z.-Y. Li, Y.-D. Yu, and J.-Z. Yu, "High-speed and broad optical bandwidth silicon modulator," *Chinese Physics B*, vol. 22, no. 11, p. 114212, nov 2013. [Online]. Available: https://doi.org/10.1088/1674-1056/22/11/114212

[88] L. Yang and J. Ding, "High-speed silicon mach–zehnder optical modulator with large optical bandwidth," *Journal of Lightwave Technology*, vol. 32, no. 5, pp. 966–970, 2014.

[89] P. Dong, X. Liu, S. Chandrasekhar, L. L. Buhl, R. Aroca, and Y.-K. Chen, "Monolithic silicon photonic integrated circuits for compact 100Gb/s coherent optical receivers and transmitters," *IEEE Journal of Selected Topics in Quantum Electronics*, vol. 20, no. 4, pp. 150–157, 2014.

[90] C. Doerr, L. Chen, T. Nielsen, R. Aroca, L. Chen, M. Banaee, S. Azemati, G. McBrien, S. Park, J. Geyer *et al.*, "O, E, S, C, and L band silicon photonics coherent modulator/receiver," in *2016 Optical Fiber Communications Conference and Exhibition (OFC)*. IEEE, 2016, pp. 1–3.

[91] Z. Yong, W. D. Sacher, Y. Huang, J. C. Mikkelsen, Y. Yang, X. Luo, P. Dumais, D. Goodwill, H. Bahrami, P. G.-Q. Lo, E. Bernier, and J. K. S. Poon, "Efficient single-drive push-pull silicon Mach-Zehnder modulators with U-shaped PN junctions for the O-band," in *2017 Optical Fiber Communications Conference and Exhibition (OFC)*, 2017, pp. 1–3.

[92] G. Zhou, L. Zhou, Y. Guo, L. Liu, L. Lu, and J. Chen, "High-efficiency silicon Mach-Zehnder modulator with U-Shaped PN junctions," in *2019 Conference on Lasers and Electro-Optics (CLEO)*, 2019, pp. 1–2.

[93] D. Petousi, L. Zimmermann, A. Gajda, M. Kroh, K. Voigt, G. Winzer, B. Tillack, and K. Petermann, "Analysis of optical and electrical tradeoffs of traveling-wave depletion-type si mach–zehnder modulators for high-speed operation," *IEEE Journal of Selected Topics in Quantum Electronics*, vol. 21, no. 4, pp. 199–206, 2015.

[94] T. Hoshida, T. Kato, D. T. Neilson, L. Galdino, V. Curri, W. Forysiak, and J. K. Fischer, "Ultra-Wideband Systems And Networks: Beyond C+L Band," *IEEE Proceedings of IEEE - UWB devices and fibers*, 2022.

[95] R. Halir, P. J. Bock, P. Cheben, A. Ortega-Moñux, C. Alonso-Ramos, J. H. Schmid, J. Lapointe, D.-X. Xu, J. G. Wangüemert-Perez, I. Molina-Fernandez, and S. Janz, "Waveguide sub-wavelength structures: a review of principles and applications," *Laser & Photonics Reviews*, vol. 9, no. 1, pp. 25–49, 2015. [Online]. Available: https://onlinelibrary.wiley.com/doi/abs/10.1002/lpor.201400083

[96] J. Kim, C. Nuzman, B. Kumar, D. Lieuwen, J. Kraus, A. Weiss, C. Lichtenwalner, A. Papazian, R. Frahm, N. Basavanhally *et al.*, "1100 x 1100 port MEMS-based optical crossconnect with 4-db maximum loss," *IEEE Photonics Technology Letters*, vol. 15, no. 11, pp. 1537–1539, 2003.

[97] D. M. Marom, D. T. Neilson, D. S. Greywall, C.-S. Pai, N. R. Basavanhally, V. A. Aksyuk, D. O. López, F. Pardo, M. E. Simon, Y. Low *et al.*, "Wavelength-selective 1 x k switches using free-space optics and MEMS micromirrors: theory, design, and implementation," *Journal of Lightwave Technology*, vol. 23, no. 4, p. 1620, 2005.

[98] G. Baxter, S. Frisken, D. Abakoumov, H. Zhou, I. Clarke, A. Bartos, and S. Poole, "Highly programmable wavelength selective switch based on liquid crystal on silicon switching elements," in *2006 Optical Fiber Communication Conference and the National Fiber Optic Engineers Conference*. IEEE, 2006, pp. 3–pp.

[99] N. K. Fontaine, R. Ryf, D. T. Neilson, and H. Chen, "Low loss wavelength selective switch with 15-THz bandwidth," in *2018 European Conference on Optical Communication (ECOC)*. IEEE, 2018, pp. 1–3.

[100] H. Chen, N. K. Fontaine, R. Ryf, B. Huang, A. Velzquez-Bentez, C. Jin, B. Ercan, and D. T. Neilson, "Wavelength selective switch for commercial multimode fiber supporting 576 spatial channels," in *ECOC 2016; 42nd European Conference on Optical Communication*. VDE, 2016, pp. 1–3.

[101] N. K. Fontaine, M. Mazur, R. Ryf, H. Chen, L. Dallachiesa, and D. T. Neilson, "36-THz bandwidth wavelength selective switch," in *2021 European Conference on Optical Communication (ECOC)*. IEEE, 2021, pp. 1–3.

[102] J.-X. Cai, H. G. Batshon, M. V. Mazurczyk, O. V. Sinkin, D. Wang, M. Paskov, W. W. Patterson, C. R. Davidson, P. C. Corbett, G. M. Wolter *et al.*, "70.46 Tb/s over 7,600 km and 71.65 Tb/s over 6,970 km transmission in C+ L band using coded modulation with hybrid constellation shaping and nonlinearity compensation," *Journal of Lightwave Technology*, vol. 36, no. 1, pp. 114–121, 2017.

[103] A. Ghazisaeidi, I. F. de Jauregui Ruiz, R. Rios-Müller, L. Schmalen, P. Tran, P. Brindel, A. C. Meseguer, Q. Hu, F. Buchali, G. Charlet, and

J. Renaudier, "Advanced C+ L-band transoceanic transmission systems based on probabilistically shaped PDM-64QAM," *Journal of Lightwave Technology*, vol. 35, no. 7, pp. 1291–1299, 2017.

[104] S. V. Firstov, V. F. Khopin, K. E. Riumkin, S. V. Alyshev, M. A. Melkumov, A. N. Guryanov, and E. M. Dianov, "Bi/Er co-doped fibers as an active medium for optical amplifiers for the C-, L-and U-telecommunication bands," in *ECOC 2016; 42nd European Conference on Optical Communication*. VDE, 2016, pp. 1–3.

[105] E. M. Dianov, "Amplification in extended transmission bands using bismuth-doped optical fibers," *Journal of Lightwave Technology*, vol. 31, no. 4, pp. 681–688, 2012.

[106] H. Ono, M. Yamada, and M. Shimizu, "S-band erbium-doped fiber amplifiers with a multistage configuration-design, characterization, and gain tilt compensation," *Journal of Lightwave Technology*, vol. 21, no. 10, p. 2240, 2003.

[107] S. Aozasa, H. Masuda, and M. Shimizu, "S-band thulium-doped fiber amplifier employing high thulium concentration doping technique," *Journal of Lightwave Technology*, vol. 24, no. 10, pp. 3842–3848, 2006.

[108] F. Hamaoka, K. Minoguchi, T. Sasai, A. Matsushita, M. Nakamura, S. Okamoto, E. Yamazaki, and Y. Kisaka, "150.3-Tb/s ultra-wideband (S, C, and L bands) single-mode fibre transmission over 40-km using ¿519Gb/s/A PDM-128QAM signals," in *2018 European Conference on Optical Communication (ECOC)*, 2018, pp. 1–3.

[109] J. W. Dawson, L. S. Kiani, P. H. Pax, G. S. Allen, D. R. Drachenberg, V. V. Khitrov, D. Chen, N. Schenkel, M. J. Cook, R. P. Crist *et al.*, "E-band Nd 3+ amplifier based on wavelength selection in an all-solid micro-structured fiber," *Optics express*, vol. 25, no. 6, pp. 6524–6538, 2017.

[110] M. Melkumov, V. Mikhailov, A. Hegai, K. Riumkin, P. Westbrook, D. DiGiovanni, and E. Dianov, "E-band data transmission over 80 km of non-zero dispersion fibre link using bismuth-doped fibre amplifier," *Electronics Letters*, vol. 53, no. 25, pp. 1661–1663, 2017.

[111] T. Sakamoto, Y. Nishida, T. Kanamori, K. Hoshino, and M. Shimizu, "1300 nm-band WDM transmission employing PDFAs," in *Optical Amplifiers and Their Applications*. Optical Society of America, 1999, p. SN2.

[112] Y. Nishida, M. Yamada, T. Kanamori, K. Kobayashi, J. Temmyo, S. Sudo, and Y. Ohishi, "Development of an efficient praseodymium-doped fiber amplifier," *IEEE journal of quantum electronics*, vol. 34, no. 8, pp. 1332–1339, 1998.

[113] M. A. Melkumov, V. Mikhailov, A. M. Khegai, K. E. Riumkin, S. V. Firstov, F. Afanasiev, A. N. Guryanov, M. Yan, Y. Sun, J. Luo *et al.*, "25 Gb s-1 data transmission using a bismuth-doped fibre amplifier with a gain peak shifted to 1300 nm," *Quantum Electronics*, vol. 48, no. 11, p. 989, 2018.

[114] V. Mikhailov, M. Melkumov, D. Inniss, A. Khegai, K. Riumkin, S. Firstov, F. Afanasiev, M. F. Yan, Y. Sun, J. Luo *et al.*, "Simple broadband bismuth doped fiber amplifier (bdfa) to extend o-band transmission reach and capacity," in *Optical Fiber Communication Conference*. Optical Society of America, 2019, pp. M1J–4.

[115] V. Mikhailov, J. Luo, D. Inniss, M. F. Yan, Y. Sun, G. S. Puc, R. S. Windeler, P. S. Westbrook, Y. Dulashko, and D. J. DiGiovanni, "Amplified transmission beyond C- and L- Bands: Bismuth doped fiber amplifier for O-band transmission Bi-doped fiber amplifiers and lasers," *Journal of Lightwave Technology, invited, DOI: 10.1109/JLT.2022.3169172*, 2022.

[116] Z. Li, A. Heidt, J. Daniel, Y. Jung, S. Alam, and D. J. Richardson, "Thulium-doped fiber amplifier for optical communications at 2 μm," *Optics Express*, vol. 21, no. 8, pp. 9289–9297, 2013.

[117] OFS, https://www.ofsoptics.com/wp-content/uploads/O-Band-Amplifier-web.pdf.

[118] J. Bromage, "Raman amplification for fiber communications systems," *Journal of Lightwave Technology*, vol. 22, no. 1, pp. 79–93, 2004.

[119] W. S. Pelouch, "Raman amplification: An enabling technology for long-haul coherent transmission systems," *Journal of Lightwave Technology*, vol. 34, no. 1, pp. 6–19, Jan 2016. [Online]. Available: http://jlt.osa.org/abstract.cfm?URI=jlt-34-1-6

[120] H. Bissessur, C. Bastide, S. Dubost, and S. Etienne, "80 × 200 Gb/s 16-QAM unrepeatered transmission over 321 km with third order Raman amplification," in *Optical Fiber Communication Conference*. Optica Publishing Group, 2015, p. W4E.2. [Online]. Available: http://opg.optica.org/abstract.cfm?URI=OFC-2015-W4E.2

[121] T. J. Xia, G. A. Wellbrock, M.-F. Huang, S. Zhang, Y.-K. Huang, D. il Chang, S. Burtsev, W. Pelouch, E. Zak, H. de Pedro, W. Szeto, and H. Fevrier, "Transmission of 400G PM-16QAM channels over long-haul distance with commercial all-distributed Raman amplification system and aged standard SMF in field," in *Optical Fiber Communication Conference*. Optica Publishing Group, 2014, p. Tu2B.1. [Online]. Available: http://opg.optica.org/abstract.cfm?URI=OFC-2014-Tu2B.1

[122] M. Islam, "Raman amplifiers for telecommunications," *IEEE Journal of Selected Topics in Quantum Electronics*, vol. 8, no. 3, pp. 548–559, 2002.

[123] L. Rapp, "Optical amplifiers for wideband optical transmission systems," in *2021 Optical Fiber Communications Conference and Exhibition (OFC)*. IEEE, 2021, pp. 1–3.

[124] R. H. Stolen and E. P. Ippen, "Raman gain in glass optical waveguides," *App. Phys. Lett.*, vol. 22, no. 6, p. 276–278, 1973.

[125] U. C. de Moura, M. A. Iqbal, M. Kamalian, L. Krzczanowicz, F. Da Ros, A. M. R. Brusin, A. Carena, W. Forysiak, S. Turitsyn, and D. Zibar, "Multi–band programmable gain Raman amplifier," *Journal of Lightwave Technology*, vol. 39, no. 2, pp. 429–438, 2021.

[126] M. Ionescu, A. Ghazisaeidi, J. Renaudier, P. Pecci, and O. Courtois, "Design optimisation of power-efficient submarine line through machine learning," in *Conference on Lasers and Electro-Optics*. Optica Publishing Group, 2020, p. STh4M.5. [Online]. Available: http://opg.optica.org/abstract.cfm?URI=CLEO_SI-2020-STh4M.5

[127] U. C. de Moura, A. M. R. Brusin, A. Carena, D. Zibar, and F. D. Ros, "Simultaneous gain profile design and noise figure prediction for Raman amplifiers using machine learning," *Opt. Lett.*, vol. 46, no. 5, pp. 1157–1160, Mar 2021. [Online]. Available: http://opg.optica.org/ol/abstract.cfm?URI=ol-46-5-1157

[128] M. Ionescu, L. Galdino, A. Edwards, J. James, W. Pelouch, E. Sillekens, D. Semrau, D. Lavery, R. I. Killey, S. Barnes, P. Bayvel, and S. Desbruslais, "91 nm C+L Hybrid Distributed Raman–Erbium-Doped Fibre Amplifier for High Capacity Subsea Transmission," in *2018 European Conference on Optical Communication (ECOC)*, 2018, pp. 1–3.

[129] M. Ionescu, D. Lavery, A. Edwards, E. Sillekens, L. Galdino, D. Semrau, R. I. Killey, W. Pelouch, S. Barnes, and P. Bayvel, "74.38 Tb/s transmission over 6300 km single mode fiber with hybrid EDFA/Raman amplifiers," in *2019 Optical Fiber Communications Conference and Exhibition (OFC)*, 2019, pp. 1–3.

[130] J. Renaudier, A. Arnould, D. Le Gac, A. Ghazisaeidi, P. Brindel, M. Makhsiyan, A. Verdier, K. Mekhazni, F. Blache, H. Debregeas, A. Boutin, N. Fontaine, D. Neilson, R. Ryf, H. Chen, M. Achouche, and G. Charlet, "107 Tb/s Transmission of 103-nm Bandwidth over 3×100 km SSMF using Ultra-Wideband Hybrid Raman/SOA Repeaters," in *2019 Optical Fiber Communications Conference and Exhibition (OFC)*, 2019, pp. 1–3.

[131] M. Ionescu, A. Arnould, D. Le Gac, S. Etienne, A. Ghazisaeidi, M. Duval, C. Bastide, H. Bissessur, and J. Renaudier, "20.6 Pb/s·km Unrepeatered Transmission without ROPA: UWB SOA Booster and Backward Raman Amplification," in *2020 European Conference on Optical Communications (ECOC)*, 2020, pp. 1–4.

[132] J. Renaudier, A. C. Meseguer, A. Ghazisaeidi, P. Tran, R. R. Muller, R. Brenot, A. Verdier, F. Blache, K. Mekhazni, B. Duval, H. Debregeas, M. Achouche, A. Boutin, F. Morin, L. Letteron, N. Fontaine, Y. Frignac, and G. Charlet, "First 100-nm Continuous-Band WDM Transmission System with 115Tb/s Transport over 100km Using Novel Ultra-Wideband Semiconductor Optical Amplifiers," in *2017 European Conference on Optical Communication (ECOC)*, 2017, pp. 1–3.

[133] O. Gautheron and M. Suyama, "Submarine cable networks," *Comptes Rendus Physique*, vol. 4, no. 1, pp. 115–126, 2003. [Online]. Available: https://www.sciencedirect.com/science/article/pii/S1631070503000069

[134] "Xtera White Paper (2021)," https://www.xtera.com/wp-content/uploads/2021/04/Raman-makes-the-Repeater-go-a-long-way.pdf.

[135] J.-X. Cai, Y. Sun, H. G. Batshon, M. Mazurczyk, H. Zhang, D. G. Foursa, and A. N. Pilipetskii, "54 Tb/s transmission over 9,150 km with optimized hybrid Raman-EDFA amplification and coded modulation," in *2014 The European Conference on Optical Communication (ECOC)*, 2014, pp. 1–3.

[136] P. Pecci, J. Ljupcho, M. Barezzani, V. Kamalov, J.-F. Marcerou, M. Cantono, M. Gumier, O. Courtois, and V. Vusirikala, "Pump farming as eabling factor to increase subsea cable capacity," *SubOptic*, vol. 4, no. 1, pp. 1–7, 2019. [Online]. Available: https://web.asn.com/media/data/files_user/72/SDM1/liens/OP14-4-PECCI-ALCATEL-SUBMARINE-NETWORKS.pdf

[137] M. A. Iqbal, L. Krzczanowicz, I. Phillips, P. Harper, and W. Forysiak, "150nm SCL-band transmission through 70km SMF using ultra-wideband dual-stage discrete Raman amplifier," in *2020 Optical Fiber Communications Conference and Exhibition (OFC)*, 2020, pp. 1–3.

[138] M. A. Iqbal, P. Harper, and W. Forysiak, "Improved design of ultra-wideband discrete Raman amplifier with low noise and high gain," in *Advanced Photonics 2018 (BGPP, IPR, NP, NOMA, Sensors, Networks, SPPCom, SOF)*. Optica Publishing Group, 2018, p. NpTh1H.2. [Online]. Available: http://opg.optica.org/abstract.cfm?URI=NP-2018-NpTh1H.2

[139] S. Liang, S. Jain, L. Xu, K. R. H. Bottrill, N. Taengnoi, M. Guasoni, P. Zhang, M. Xiao, Q. Kang, Y. Jung, P. Petropoulos, and D. J. Richardson, "High gain, low noise, spectral-gain-controlled, broadband lumped fiber Raman amplifier," *Journal of Lightwave Technology*, vol. 39, no. 5, pp. 1458–1463, 2021.

[140] M. A. Iqbal, L. Krzczanowicz, I. D. Philips, P. Harper, and W. Forysiak, "Noise performance improvement of broadband discrete Raman amplifiers using dual stage distributed pumping architecture," *Journal of Lightwave Technology*, vol. 37, no. 14, pp. 3665–3671, 2019.

[141] M. A. Iqbal, M. A. Z. Al-Khateeb, L. Krzczanowicz, I. D. Phillips, P. Harper, and W. Forysiak, "Linear and nonlinear noise characterisation of dual stage broadband discrete Raman amplifiers," *Journal of Lightwave Technology*, vol. 37, no. 14, pp. 3679–3688, 2019.

[142] L. Krzczanowicz, M. A. Z. Al-Khateeb, M. A. Iqbal, I. Phillips, P. Harper, and W. Forysiak, "Performance estimation of discrete Raman amplification within broadband optical networks," in *2019 Optical Fiber Communications Conference and Exhibition (OFC)*, 2019, pp. 1–3.

[143] L. Krzczanowicz, M. A. Iqbal, I. Phillips, P. Harper, and W. Forysiak, "High-capacity multi-span transmission performance characterization of broadband discrete Raman amplifier," *Opt. Express*, vol. 28, no. 12, pp. 18 296–18 303, Jun 2020. [Online]. Available: http://opg.optica.org/oe/abstract.cfm?URI=oe-28-12-18296

[144] A. Ghazisaeidi, F. Vacondio, A. Bononi, and L. A. Rusch, "SOA intensity noise suppression in spectrum sliced systems: A multicanonical Monte Carlo simulator of extremely low BER," *Journal of Lightwave Technology*, vol. 27, no. 14, pp. 2667–2677, 2009.

[145] M. J. Connelly, *Semiconductor optical amplifiers*. Springer Science & Business Media, 2007.

[146] A. D. McCoy, P. Horak, B. C. Thomsen, M. Ibsen, and D. J. Richardson, "Noise suppression of incoherent light using a gain-saturated SOA: Implications for spectrum-sliced WDM systems," *Journal of Lightwave Technology*, vol. 23, no. 8, pp. 2399–2409, 2005.

[147] F. Ohman, S. Bischoff, B. Tromborg, and J. Mork, "Noise and regeneration in semiconductor waveguides with saturable gain and absorption," *IEEE journal of quantum electronics*, vol. 40, no. 3, pp. 245–255, 2004.

[148] M. Shtaif, B. Tromborg, and G. Eisenstein, "Noise spectra of semiconductor optical amplifiers: Relation between semiclassical and quantum descriptions," *IEEE journal of quantum electronics*, vol. 34, no. 5, pp. 869–878, 1998.

[149] O. Leclerc, B. Lavigne, E. Balmefrezol, P. Brindel, L. Pierre, D. Rouvillain, and F. Seguineau, "Optical regeneration at 40 gb/s and beyond," *Journal of Lightwave Technology*, vol. 21, no. 11, p. 2779, 2003.

[150] K. Morito, S. Tanaka, S. Tomabechi, and A. Kuramata, "A broadband MQW semiconductor optical amplifier with high saturation output power and low noise figure," *IEEE photonics technology letters*, vol. 17, no. 5, pp. 974–976, 2005.

[151] H. Carrère, V. Truong, X. Marie, R. Brenot, G. De Valicourt, F. Lelarge, and T. Amand, "Large optical bandwidth and polarization insensitive semiconductor optical amplifiers using strained InGaAsP quantum wells," *Applied Physics Letters*, vol. 97, no. 12, p. 121101, 2010.

[152] A. Verdier, A. C. Meseguer, K. Mekhazni, F. Blache, C. Calo, M. Goix, B. Duval, C. Fortin, F. Martin, C. Gomez *et al.*, "Wideband material for low linewidth widely tunable laser and reach extender for optical access networks," in *2017 European Conference on Optical Communication (ECOC)*. IEEE, 2017, pp. 1–3.

[153] T. Akiyama, M. Ekawa, M. Sugawara, K. Kawaguchi, H. Sudo, A. Kuramata, H. Ebe, and Y. Arakawa, "An ultrawide-band semiconductor optical amplifier having an extremely high penalty-free output power of 23 dbm achieved with quantum dots," *IEEE Photonics Technology Letters*, vol. 17, no. 8, pp. 1614–1616, 2005.

[154] J. Renaudier, A. Arnould, A. Ghazisaeidi, D. Le Gac, P. Brindel, E. Awwad, M. Makhsiyan, K. Mekhazni, F. Blache, A. Boutin *et al.*, "Recent advances in 100+ nm ultra-wideband fiber-optic transmission systems using semiconductor optical amplifiers," *Journal of Lightwave Technology*, vol. 38, no. 5, pp. 1071–1079, 2020.

[155] L. H. Spiekman, J. Wiesenfeld, A. Gnauck, L. Garrett, G. Van Den Hoven, T. Van Dongen, M. Sander-Jochem, and J. Binsma, "Transmission of 8 DWDM channels at 20 Gb/s over 160 km of standard fiber using a cascade of semiconductor optical amplifiers," *IEEE Photonics Technology Letters*, vol. 12, no. 6, pp. 717–719, 2000.

[156] H. Kim, S. Chandrasekhar, A. Srivastava, C. Burrus, and L. Buhl, "10 Gbit/s based WDM signal transmission over 500 km of NZDSF using semiconductor optical amplifier as the in-line amplifier," *Electronics Letters*, vol. 37, no. 3, pp. 185–187, 2001.

[157] E. Ciaramella, A. D'Errico, V. Donzella, G. Contestabile, S. Betti, V. Carrozzo, F. Curti, and M. Guglielmucci, "In-field WDM-DPSK 8× 10 Gb/s transmission over 300 km using four common SOAs," in *National Fiber Optic Engineers Conference*. Optical Society of America, 2007, p. JThA75.

[158] K. Morito, M. Ekawa, T. Watanabe, and Y. Kotaki, "High-output-power polarization-insensitive semiconductor optical amplifier," *Journal of Lightwave Technology*, vol. 21, no. 1, pp. 176–181, 2003.

[159] W. Loh, J. J. Plant, J. Klamkin, J. P. Donnelly, F. J. O'Donnell, R. J. Ram, and P. W. Juodawlkis, "Noise figure of Watt-class ultralow-confinement semiconductor optical amplifiers," *IEEE Journal of Quantum Electronics*, vol. 47, no. 1, pp. 66–75, 2010.

[160] P. W. Juodawlkis, J. J. Plant, W. Loh, L. J. Missaggia, F. J. O'Donnell, D. C. Oakley, A. Napoleone, J. Klamkin, J. T. Gopinath, D. J. Ripin *et al.*, "High-power, low-noise 1.5-μm slab-coupled optical waveguide (scow) emitters: physics, devices, and applications," *IEEE Journal of Selected Topics in Quantum Electronics*, vol. 17, no. 6, pp. 1698–1714, 2011.

[161] A. Arnould, D. Le Gac, A. Ghazisaeidi, P. Brindel, M. Makhsiyan, K. Mekhazni, F. Blache, H. Debregeas, M. Achouche, G. Charlet *et al.*, "Impact of the number of channels on the induced nonlinear distortions in ultra-wideband SOAs," in *Optical Fiber Communication Conference*. Optical Society of America, 2019, pp. Tu3F–1.

[162] A. Ghazisaeidi, "Theory of coherent WDM systems using in-line semiconductor optical amplifiers," *Journal of Lightwave Technology*, vol. 37, no. 17, pp. 4188–4200, 2019.

[163] J. Renaudier and A. Ghazisaeidi, "Scaling capacity growth of fiber-optic transmission systems using 100+ nm ultra-wideband semiconductor optical amplifiers," *Journal of Lightwave Technology*, vol. 37, no. 8, pp. 1831–1838, 2019.

[164] L. Tiemeijer, P. Thijs, T. Van Dongen, J. Binsma, E. Jansen, S. Walczyk, G. Van Den Hoven, and E. Pennings, "High-gain, high-power 1550-nm polarization independent MQW optical amplifier," *IEEE Photonics Technology Letters*, vol. 8, no. 9, pp. 1142–1144, 1996.

[165] K. Morito and S. Tanaka, "Record high saturation power (+ 22 dBm) and low noise figure (5.7 dB) polarization-insensitive SOA module," *IEEE photonics technology letters*, vol. 17, no. 6, pp. 1298–1300, 2005.

[166] J. Renaudier, A. C. Meseguer, A. Ghazisaeidi, P. Tran, R. R. Muller, R. Brenot, A. Verdier, F. Blache, K. Mekhazni, B. Duval *et al.*, "First 100-nm continuous-band WDM transmission system with 115Tb/s transport over 100km using novel ultra-wideband semiconductor optical amplifiers," in *2017 European Conference on Optical Communication (ECOC)*. IEEE, 2017, pp. 1–3.

[167] J. Renaudier, A. Arnould, D. Le Gac, A. Ghazisaeidi, P. Brindel, M. Makhsiyan, A. Verdier, K. Mekhazni, F. Blache, H. Debregeas *et al.*, "107 Tb/s transmission of 103-nm bandwidth over 3× 100 km SSMF using ultra-wideband hybrid Raman/SOA repeaters," in *Optical Fiber Communication Conference*. Optical Society of America, 2019, pp. Tu3F–2.

[168] J. Renaudier, A. C. Meseguer, A. Ghazisaeidi, P. Brindel, P. Tran, A. Verdier, F. Blache, M. Makhsiyan, K. Mekhazni, C. Calo *et al.*, "Field trial of 100nm ultra-wideband optical transport with 42GBd 16QAM real-time and 64GBd PCS64QAM channels," in *2018 European Conference on Optical Communication (ECOC)*. IEEE, 2018, pp. 1–3.

[169] H. Carrère and X. Marie, "Band structure engineering of semiconductor devices for optical telecommunications," *Semiconductor Modeling Techniques, Springer*, pp. 153–194, 2012.

[170] M. Ohashi, K. Shiraki, and K. Tajima, "Optical loss property of silica-based single-mode fibers," *Journal of Lightwave Technology*, vol. 10, no. 5, pp. 539–543, 1992.

[171] G. T. Jasion, T. D. Bradley, K. Harrington, H. Sakr, Y. Chen, E. N. Fokoua, I. A. Davidson, A. Taranta, J. R. Hayes, D. J. Richardson *et al.*, "Hollow core NANF with 0.28 dB/km attenuation in the C and L bands," in *Optical Fiber Communication Conference*. Optical Society of America, 2020, pp. Th4B–4.

[172] W. Belardi, "Design and properties of hollow antiresonant fibers for the visible and near infrared spectral range," *Journal of Lightwave Technology*, vol. 33, no. 21, pp. 4497–4503, 2015.

[173] T. D. Bradley, J. R. Hayes, Y. Chen, G. T. Jasion, S. R. Sandoghchi, R. Slavík, E. N. Fokoua, S. Bawn, H. Sakr, I. A. Davidson *et al.*, "Record low-loss 1.3 db/km data transmitting antiresonant hollow

core fibre," in *2018 European Conference on Optical Communication (ECOC)*. IEEE, 2018, pp. 1–3.

[174] H. Sakr *et al.*, "Hollow core NANFs with five nested tubes and record low loss at 850, 1060, 1300 and 1625nm," in *Optical Fiber Communication Conference*. Optical Society of America, 2021, pp. post–deadline paper F3A.4.

[175] G. T. Jasion, H. Sakr, J. R. Hayes, S. R. Sandoghchi, L. Hooper *et al.*, "0.174 dB/km hollow core double nested antiresonant nodeless fiber (DNANF)," in *2022 Optical Fiber Communications Conference and Exhibition (OFC)*, 2022, pp. 1–3.

[176] F. Poletti, "Nested antiresonant nodeless hollow core fiber," *Optics express*, vol. 22, no. 20, pp. 23 807–23 828, 2014.

[177] A. Nespola *et al.*, "Ultra-long-haul WDM transmission in a reduced inter-modal interference NANF hollow-core fiber," in *Optical Fiber Communication Conference*. Optical Society of America, 2021, pp. post–deadline paper F3B.5.

[178] Y. Tamura, H. Sakuma, K. Morita, M. Suzuki, Y. Yamamoto, K. Shimada, Y. Honma, K. Sohma, T. Fujii, and T. Hasegawa, "The first 0.14-dB/km loss optical fiber and its impact on submarine transmission," *Journal of Lightwave Technology*, vol. 36, no. 1, pp. 44–49, 2018.

[179] A. Nespola, S. Straullu, T. D. Bradley, H. C. Mulvad, J. R. Hayes *et al.*, "Record PM-16QAM and PM-QPSK transmission distance (125 and 340 km) over hollow-core-fiber," in *2019 European Conference on Optical Communication (ECOC)*, 2019, pp. 1–3.

[180] A. Nespola, S. Straullu, T. D. Bradley, K. Harrington, H. Sakr, G. T. Jasion, E. N. Fokoua, Y. Jung, Y. Chen, J. R. Hayes *et al.*, "Transmission of 61 C-Band channels over record distance of hollow-core-fiber with L-Band interferers," *Journal of Lightwave Technology*, vol. 39, no. 3, pp. 813–820, 2021.

[181] P. Poggiolini and F. Poletti, "Opportunities and challenges for long-distance transmission in hollow-core fibres," *Journal of Lightwave Technology*, vol. 40, no. 6, pp. 1605–1616, 2022.

[182] T. Hoshida, V. Curri, L. Galdino, D. T. Neilson, W. Forysiak, J. K. Fischer, T. Kato, and P. Poggiolini, "Ultra-wideband systems and networks: beyond C+L-band," *Proceedings of the IEEE, to be published*, 2022.